Geostrophic Regimes, Intermediate Solitary Vortices and Jovian Eddies

GARETH P. WILLIAMS

Geophysical Fluid Dynamics Laboratory/NOAA, Princeton University, Princeton, NJ 08540

TOSHIO YAMAGATA[1]

Geophysical Fluid Dynamics Program, Princeton University, Princeton, NJ 08540

(Manuscript received 12 April 1983, in final form 25 October 1983)

ABSTRACT

We examine the relevance to Jupiter's atmosphere of the solitary vortices favored at scales intermediate to those of the quasi-geostrophic (QG) and planetary-geostrophic motions. Horizontal divergence plays a crucial role in the intermediate-geostrophic (IG) dynamics and leads to asymmetries in vortex behavior; in particular, anticyclonic vortices are generally more stable than cyclonic vortices when the mean flow is weak or westerly. The IG vortices always propagate westward at close to the planetary long-wave speed, regardless of the mean zonal flow. Meridional shear influences only secondary aspects of vortex behavior. Although governed by a form of the Korteweg-deVries (KdV) equation, vortex encounters produce coalescence not soliton behavior.

Jupiter's Great Red Spot and Large Ovals appear to be in, or close to, an IG balance while the Small Ovals lie in a QG balance. The stability of anticyclonic IG vortices may explain why most of Jupiter's super-eddies prefer anticyclonic spin. Solutions to the shallow water (SW) equations, using Jovian parameters, show that an IG vortex with the scale and environment of the Great Red Spot has great longevity and that such a vortex may originate in a weak barotropic instability of the zonal currents. Strong barotropic instability on the IG scale differs from its counterpart on the QG scale and produces multiple, steep, isolated vortices resembling the Large Ovals.

Equations are derived for all forms of geostrophic balance (three basic classes, ten subsets) to investigate the uniqueness of the IG system. Numerical studies use the IG β-plane equation to examine basic modal properties and the full SW equations to examine the Jovian eddies.

1. Introduction

Jupiter's atmosphere displays many forms of motion, some coherent and long-lived, others irregular and transient. The ubiquitous waves and turbulence occur on the smaller scale, the steady zonal currents on the larger scale, while the Great Red Spot (GRS), the Large Ovals, the tropical plumes and the late South Tropical Disturbance (1901–39) occur on the intermediate scale. Because of their vastly different sizes, the various eddies probably lie in different dynamical regimes.[2] As with oceanic eddies, motions at the intermediate scale are the least understood.

Jovian motions are believed to have much in common with those of the ocean: a strong energy conversion by the small eddies, activity over a wide range of scales, a weak dissipation, coherent and turbulent structuring, and similar nondimensional parameter ranges (Williams, 1978). Differences occur not so much in the basic modes of motion but rather in their forcing mechanisms and boundary conditions. The efficacy of the ocean–Jupiter analog in understanding the Jovian planetary circulation and turbulence suggests that it might also be useful to look for correspondences between the coherent eddy forms of the two systems.

Three classes of ocean dynamics are known: the quasi-geostrophic (QG), the planetary-geostrophic[3] (PG) and the recently discovered intermediate geostrophic (IG) (Charney and Flierl, 1981; Yamagata, 1982). They govern the small, large and medium scales of motion, respectively. These regimes are more distinct in the ocean and in Jupiter's atmosphere than in Earth's atmosphere, because a greater scale separation exists in those systems. The Jovian QG modes have been discussed with respect to the problems of the generation of multiple jets by baroclinic eddies (Williams 1979a; Williams and Holloway, 1982) and the generation of planetary solitons by zonal wind shear (Maxworthy and Redekopp, 1976).

The only IG processes known at present are those associated with a class of remarkably stable solitary vortices that are the intrinsic modes of the shallow

[1] Permanent affiliation: Research Institute for Applied Mechanics, Kyushu University, 87, Kasuga 816, Japan.

[2] See Section 3 for a detailed scale analysis and Hunt and Moore (1981) for a convenient description of the various Jovian phenomena.

[3] Called Geostrophy of Type 2 by Phillips (1963).

water (SW) equations in a certain parameter range. These vortices were developed for oceanic models and applied to tropical coastal eddies (Matsuura and Yamagata, 1982). Our purpose in this paper is to see if they have some bearing on the structure and stability of Jupiter's Great Red Spot and Large Ovals. Other vortex theories have been applied to the various Jovian eddies but have encountered the difficulties noted below.

The Rossby shear-soliton theory (Maxworthy and Redekopp, 1976) and the singular vortex model (Ingersoll and Cuong, 1981) are both based on approximations to the QG equations. Thus, their solutions relate to eddies of only the smallest planetary scale—no greater than that of the Small Ovals[4] (see Section 3)—and their vortices must compete and coexist with other QG processes. The turbulent nature of the smaller Jovian eddies probably prevents solitons or singular vortices from existing in their range of scales.

The non-oval shape and the 40 m s^{-1} westward drift of Rossby shear-solitons are features that are not seen for any Jovian eddy (Beaumont, 1980). There is also some question as to whether the QG approximation remains valid for nonlinear phenomena, such as solitons, whose longitudinal scale greatly exceeds their latitudinal one (Yamagata, 1980, 1982). Doubts have also arisen as to how stable and significant the "steadying" vortex found by Ingersoll and Cuong really is, since: 1) it is generated at a large Froude number, even though the QG equations are only valid for values near unity, 2) it is nearly as large as the computational domain and may be relaxing toward a normal mode of the type discussed by Kuo (1959), 3) it is a restricted quasilinear vortex—because of the use of a linear integration function—and may be composed of permanent linear waves of the type discussed by Thompson (1948). This model also depends crucially on the assumption that the vertical scale of the eddies is much smaller than that of the mean flow. This hypothesis is based on the belief that the steadiness of Jupiter's jets implies vertically shallow eddies. However, steady jets can occur whenever the eddies are horizontally small, so vertical complexity is not required for, nor justified by, the form of the planetary circulation.

In the following sections, we discuss a form of solitary vortex that is a highly stable fundamental nonlinear mode, that is strongly isolated (both parametrically and spatially) and can exist in almost any mean flow in a simple model atmosphere. Unlike the Rossby shear-soliton it can exist without any meridional shear. We begin, in Section 2, with the derivation and discussion of the various dynamical regimes and their equations; this reveals the uniqueness of the IG system. Then, in Section 3, we examine the parametric range of the various Jovian eddies and try to categorize them. In Section 4, the IG equations are solved numerically, to illustrate the basic properties of solitary vortices on a β-plane. In Section 5, we solve the full SW equations, on a sphere, to see whether the IG solitary vortex can exist and remain stable when other dynamical modes (e.g., QG) also occur. These calculations are made with Jovian parameter values to determine whether stable IG vortices with the characteristics of the GRS and Large Ovals can be generated under "planetary" conditions. We also try to create IG vortices *ab initio*, by perturbing barotropically unstable zonal jets, to test ideas about the origin of the Great Red Spot and Large Ovals.

2. Geostrophic regimes and the intermediate-geostrophic equations

a. Basic model

The shallow water equations give the simplest representation of stratified planetary-scale motions. This model can be interpreted either as a single layer acting under external gravity or as two layers, one of which is much deeper, acting under a reduced (or internal) gravity. On a β-plane, the equations are

$$\left.\begin{aligned} &\frac{Du}{Dt} - (f_0 + \beta y)v = -g\eta_x \\ &\frac{Dv}{Dt} + (f_0 + \beta y)u = -g\eta_y \\ &\frac{D\eta}{Dt} + (H + \eta)(u_x + v_y) = 0 \\ &\frac{D(\ \ )}{Dt} \equiv (\ \ )_t + u(\ \ )_x + v(\ \ )_y \end{aligned}\right\}, \tag{2.1}$$

where η measures the displacement of the surface from the mean layer thickness H, g is the internal or external gravity and $x = a\lambda \cos\theta_0$, $y = a(\theta - \theta_0)$ are the β-plane coordinates based on the longitude and central latitude (λ, θ_0) and (u, v) the corresponding velocity components. The Coriolis terms $f_0 = 2\Omega \sin\theta_0$, $\beta = 2\Omega \cos\theta_0/a$ are for a planet of radius a and rotation rate Ω.

b. Nondimensional equations

For planetary motions, the appropriate scale factors[5] for the $\mathbf{u}$, x, t, η variables are U, L, $L/\beta L_R^2$, LUf_0/g, where $L_R = c_g/f_0$ is the deformation radius and $c_g = (gH)^{1/2}$ the internal or external gravity long-wave speed. Inserting these into (2.1) gives the nondimensional equations

[4] The Great Red Spot is much too large to be a Rossby shear-soliton. For a further critique of these theories, see Flierl *et al.* (1983).

[5] We assume that processes are essentially isotropic in x and y.

$$\left.\begin{aligned} \hat{\beta}\hat{s}\frac{Du}{Dt} - (1+\hat{\beta}y)v &= -\eta_x \\ \hat{\beta}\hat{s}\frac{Dv}{Dt} + (1+\hat{\beta}y)u &= -\eta_y \\ \hat{\beta}\frac{D\eta}{Dt} + \left(1+\frac{\hat{\epsilon}}{\hat{s}}\eta\right)(u_x+v_y) &= 0 \\ \frac{D(\ )}{Dt} \equiv (\ )_t + \frac{\hat{\epsilon}}{\hat{\beta}\hat{s}}[u(\ )_x + v(\ )_y] & \end{aligned}\right\}, \quad (2.2)$$

where $\hat{\beta} = \beta L/f_0$, $\hat{\epsilon} = U/Lf_0$, $\hat{s} = L_R^2/L^2$ are the nondimensional sphericity, Rossby and stratification parameters. These equations can be combined into an expression for the conservation of potential vorticity:

$$\left.\begin{aligned} \frac{D\Pi}{Dt} &= 0 \\ \Pi &= (1+\hat{\beta}y+\hat{\epsilon}\zeta)/(1+\hat{\epsilon}\hat{s}^{-1}\eta) \end{aligned}\right\}, \quad (2.3)$$

where

$$\zeta = v_x - u_y.$$

c. Dynamical regimes

The types of motion exhibited by this model depend on the parameter range in question. There are three basic classes of motion: the QG, PG and IG (cf. Gent and McWilliams, 1983). The best known balances occur at the smallest planetary scales ($L \sim L_R \ll a$), where $\hat{\epsilon} \sim \hat{\beta} \ll 1$ and $\hat{s} \sim 1$ reduce Eqs. (2.2) and (2.3) to the quasi-geostrophic system and at the largest planetary scales ($L \sim a \gg L_R$), where $\hat{\epsilon} \sim \hat{s} \ll 1$ and $\hat{\beta} \to 1$ give the planetary-geostrophic system.[6] We are particularly interested in the motions that lie between those two extremes, motions that involve both the QG wave dispersion and the PG nonlinear divergence effects. At these scales ($L_R < L < a$), the parameters $\hat{\epsilon}$, $\hat{s}$, $\hat{\beta}$ are all small (but to a different degree), and the motions are governed by the IG equation (Charney and Flierl, 1981; Yamagata, 1982).

To derive the IG equation, the major nonlinear terms in Eq. (2.2) must be included. These terms become important, with respect to linear wave effects, whenever some of the factors $\hat{\epsilon}$, $\hat{\epsilon}/\hat{\beta}$, $\hat{\epsilon}/\hat{s}\hat{\beta}$ approach unity. At the intermediate scales, this occurs when the parameters have the following related degrees of smallness:

$$\hat{\beta} \ll 1, \quad \hat{\epsilon} = E\hat{\beta}^2, \quad \hat{s} = S\hat{\beta}, \quad (2.4)$$

where E, S are numbers of O(1). If we use this relationship to expand (2.2) and (2.3) in powers of $\hat{\beta}$, we obtain the IG equation (see Section 2d for details).

[6] The β-plane approximation is not strictly valid for the largest planetary scales. However, our analysis and use of the constraint $\hat{\beta} < 1$ yields a β-plane representation of these modes, one that captures the essence of their behavior.

The reduction in parametric freedom introduced by Eq. (2.4) occurs because we are defining *balances* between various processes, not the processes themselves, and parameter *ratios* determine these. Physical relationships such as that implied by (2.4) must be selected to make the basic equations tractable; we cannot expand in powers of all three basic parameters. For our planetary problems, $\hat{\beta}$ is the basic parameter because linear planetary wave dispersion is the main mechanism against which the nonlinear effects are measured.[7]

If we assume a more general parametric relationship of the form $\hat{\epsilon} = E\hat{\beta}^n$, $\hat{s} = S\hat{\beta}^m$, the complete set of dynamical systems (in the geostrophic regime) can be determined on taking $n = 1$–4 and $m = 0$–3 (see Table 1). The equation derivations resemble that for the IG system in Section 2d. From Table 1 we see that the geostrophic regime consists basically of QG, PG and IG regions, with three QG and six PG parametric subranges—the most important of which lie in the top left corner. We classify a region as QG if dispersion dominates, as PG if nonlinear[8] divergence dominates, and as IG if both dispersion and nonlinear divergence are present. As Table 1 clearly illustrates, there is only one parametric region where all the processes are active; this gives the unique IG system. At higher powers of $\hat{\beta}$, the same equations reappear so the tabulation is complete.

The following highlights of the different subranges of Table 1 should be noted.

1) QG_0: This is the classical quasi-geostrophic system. It is strongly nonlinear (advective) and dispersive and governs such phenomena as cyclones, MODE eddies, modons and Small Ovals.

2) QG_1: This is the traditional linear quasi-geostrophic system (with divergence) used for the analysis of Rossby waves.

3) QG_2: The linear divergence effect, not vorticity, defines this dispersive Rossby wave regime. The meridional twisting term distorts the waves.

4) PG_0: This is the β-plane representation of the classical planetary-geostrophic (Burger[9]) system. It is strongly nonlinear (from divergence) and nondispersive. A long planetary wave or Sverdrup balance can occur when $E' \ll 1$.

5) PG_1: This is the basic nonlinear (divergence) PG balance. Unlike PG_0, waves do not occur.

6) PG_2: This is similar to PG_0 with modifications by the nonlinear advection terms; strong velocities are present. Gulf Stream Rings may be in this subrange during their decay stage.

[7] This analysis does not apply to f_0-plane motions.

[8] PG_5 is a degenerate, linear case.

[9] Not to be confused with J. Burgers' turbulence model, even though the equations are similar. Note also that, although $\hat{\beta} \sim 1$ in the original Burger analysis, a large value of this parameter is not necessary for the nonlinear divergence to be important.

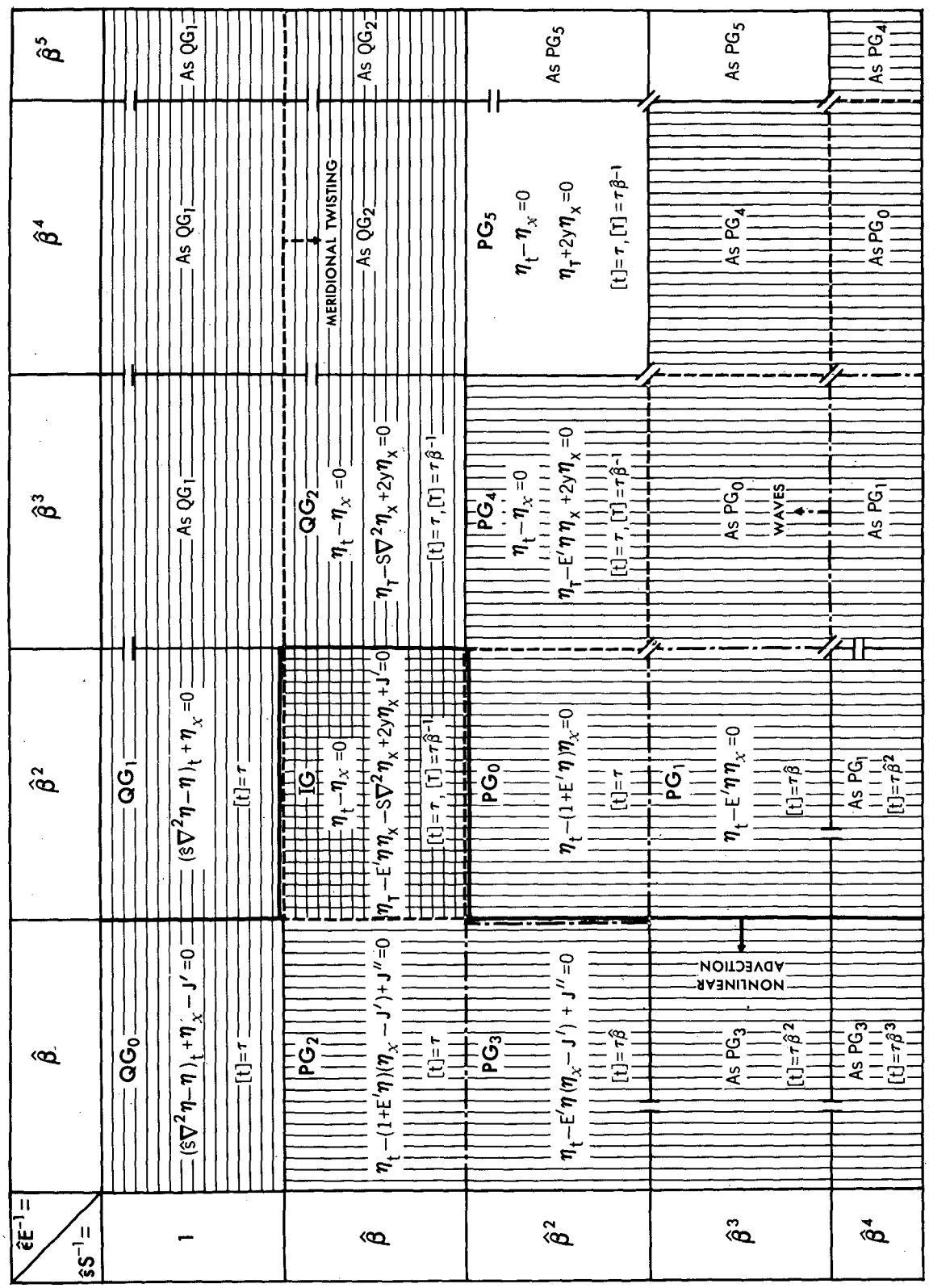

TABLE 1. The dynamical regimes of geostrophic flow. The governing equations are shown as a function of the basic parameters $\hat{\epsilon}$ and $\hat{s}$, which are expressed in decreasing values (from top left) as powers of $\hat{\beta}$, where $\hat{\beta} \ll 1$. QG_n denotes a quasi-geostrophic balance (dispersion dominates), PG_n a planetary-geostrophic balance (nonlinear divergence dominates) and IG an intermediate-geostrophic balance (all processes present but weak). Where two equations occur, the first describes the strong, fast changes and the second describes the slow, weak changes (see Section 2d). Vertical and horizontal shading indicates the regions where nonlinear divergence and dispersion prevail, respectively. Additional boundaries denote transitions from activity to inactivity for the nonlinear advection, meridional twisting and all waves. Notation: $\tau = (f_0\delta\beta)^{-1}$ is the basic time scale; $[t]$ and $[T]$ are the time scales for t and T; $X = x + t$, $E' = ES^{-1}$, $J' = E^2S^{-1}[(\eta_y^2 - \eta_x^2)\eta_{xy} + (\eta_{xx} - \eta_{yy})\eta_x\eta_y]$.

7) PG_3: This is similar to PG_1 but with modifications by nonlinear advection terms.

8) PG_4: This is similar to PG_0, with nondispersive waves modified by a weak nonlinear (divergence) steepening and a weak meridional twisting.

9) PG_5: This is similar to PG_4 but without the nonlinear term. It is a degenerate form.

10) IG: This is the one and only intermediate-geostrophic region. The basic balance is between a weak nonlinear (divergence) steepening and a weak wave dispersion, with modifications by the nonlinear advection and the meridional twisting. Possible examples are the Costa Rican gyres, the Great Red Spot and the Large Ovals.

Although separate QG, PG and IG forms of motion can occur simultaneously in a system whose energy is spread over a wide range of scales, it is unlikely that scale discretization and isolation is sufficient to give motions in more than one of the various subranges of the QG and PG regimes. The special properties of the IG system—its distinct scales, its intermediate parametric location and its fundamental (solitary vortex) modes—give it a high chance of occurring in multiscale motions.

d. Intermediate equations

To derive the IG equations, we must first extract the geostrophic balance

$$u^g = -\eta_y, \quad v^g = +\eta_x, \tag{2.5}$$

from Eqs. (2.2). The ageostrophic velocities $\mathbf{u}^a = \mathbf{u} - \mathbf{u}^g$ then satisfy

$$\left.\begin{aligned} (1+\hat{\beta}y)u^a &= -\hat{\beta}\hat{s}\frac{Dv}{Dt} - \hat{\beta}yu^g \\ (1+\hat{\beta}y)v^a &= \hat{\beta}\hat{s}\frac{Du}{Dt} - \hat{\beta}yv^g \\ (\hat{s}+\hat{\epsilon}\hat{\eta})(u^a_x + v^a_y) &= -\hat{\beta}\hat{s}\frac{D\eta}{Dt} \end{aligned}\right\}. \tag{2.6}$$

For the IG parameter relationships of Eq. (2.4), Eqs. (2.6) and (2.3) approximate to

$$\left.\begin{aligned} u^a &= -\hat{\beta}yu^g + O(\hat{\beta}^2) \\ v^a &= -\hat{\beta}yv^g + O(\hat{\beta}^2) \\ \Pi &= 1 + \hat{\beta}(y - ES^{-1}\eta) \\ &\quad + \hat{\beta}^2(E\zeta - ES^{-1}y\eta + E^2S^{-2}\eta^2) + O(\hat{\beta}^3) \end{aligned}\right\}. \tag{2.7}$$

Substituting (2.5) and (2.7) into (2.3) gives to $O(\hat{\beta})$:

$$\eta_t - \eta_x = 0, \tag{2.8}$$

the equation for nondispersive planetary eddies. Solutions exist in the form $\eta = \eta(X, y, T)$ where $X = x + t$ denotes a coordinate traveling westward with the planetary long-wave speed, and where $T = \hat{\beta}t$ denotes the strained (slow) time coordinate that describes long-term evolution. At this level of approximation, no interaction occurs between the mean zonal flow and the eddies,[10] which always move westward (cf. White, 1977).

The $O(\hat{\beta}^2)$ terms in (2.3) give the prediction equation for the slow changes:

$$\underset{\text{(i)}}{\eta_T} - \underset{\text{(ii)}}{ES^{-1}\eta\eta_X} - \underset{\text{(iii)}}{S\nabla^2\eta_X} + \underset{\text{(iv)}}{2y\eta_X} + \underset{\text{(v)}}{EJ(\nabla^2\eta, \eta)} = 0, \tag{2.9}$$

where $J(A, B) \equiv A_XB_y - A_yB_X$, $\nabla^2(\ ) \equiv (\ )_{XX} + (\ )_{yy}$. The local vorticity time change ζ_T does not appear in this equation as it is negligible compared to term (i) when $L \gg L_R$. [The same is true for the QG potential vorticity $(\nabla^2\eta - \hat{s}^{-1}\eta)$; the second term dominates when $\hat{s} \ll 1$.] Term (ii) describes the ageostrophic divergence and stems from the last two terms of Π in Eq. (2.7); the nonlinearity measures the finite amplitude changes in thickness (cf. Anderson and Kilworth, 1979). Term (iii) is the planetary wave dispersion, term (iv) the meridional twisting of the long waves (cf. Meyers, 1979) and term (v), the geostrophic advection of vorticity.

The divergence term (ii) and, to a lesser extent, term (iv) make Eq. (2.9) asymmetric with respect to cyclonic and anticyclonic eddies. For anticyclones, the nonlinear steepening of term (ii) can balance the wave dispersion of term (iii), especially in the absence of mean flows, and allow long-lived vortices. This nonlinear steepening is due to the movement of the surface and not to the advection of momentum—the steepening process involved in QG solitons. For cyclones, terms (ii) and (iii) are the same sign and must be balanced by term (i), leading to the dispersion of the vortex. Term (v) is small, except during vortex collisions, and term (iv) is small except when the eddies are of domain size.

For the IG and PG approximations, only one quadratic quantity (η^2), the potential energy, obeys a conservation equation, whereas the basic equations and the QG approximation conserve both total energy and potential enstrophy. Thus, the two-dimensional and QG forms of turbulent cascade cannot occur at the IG and PG scales.

e. Mean flow effects

To examine the asymmetric behavior of (2.9) when zonal currents $u^0(y)$ are present, we define the new dependent variable

$$\xi = \eta + \int_0^y u^0(y')dy', \tag{2.10}$$

[10] If they have the same vertical structure.

and substitute it into (2.9). This gives

$$\xi_T - ES^{-1}\xi\xi_X - (S + Eu^0)\nabla^2\xi_X + \Big[2y + Eu^0_{yy} + ES^{-1}\int_0^y u^0(y')dy'\Big]\xi_X + EJ(\nabla^2\xi, \xi) = 0. \quad (2.11)$$

Three types of solution can occur depending on the sign of the third term:

- $S + Eu^0 > 0$. Eddies behave as for $u^0 = 0$ (see Section 2d); only anticyclones are long-lived, with the dispersive effect (third term) balancing the nonlinear steepening (second term).
- $S + Eu^0 < 0$. Only cyclonic eddies are long-lived. The balance is the same as in the first solution.
- $S + Eu^0 = 0$. Both cyclonic and anticyclonic eddies are long-lived when u^0 has this unique value. Critical layers surround the vortex and contain its energy. A weak nonlinear steepening now balances a weak nonlinear advection (last term).

f. Numerical methods

We carry out two sets of numerical studies. First, we solve the IG β-plane equation (2.9) using standard centered differencing and the Arakawa (1966) scheme for the Jacobian term, even though energy and enstrophy constraints are not needed. The method for the nonlinear term (ii) conserves η and η^2. To avoid boundary effects, we chose a channel that is wide in both X and y, setting $y = \pm 10$, $X = \pm 10$. Boundary conditions are periodic in X and freeslip in y. The resolution is 64×64. Time smoothing by the restart method (every 20 steps) controls computational modes.

Second, we solve the full shallow water equations on a sphere:

$$u_t + \mathbf{V}\cdot\nabla u - (f + ua^{-1}\tan\theta)v = -\frac{(gh)_\lambda}{a\cos\theta} + \frac{1}{\tau}(u_J - u) + \nu\nabla^2 u, \quad (2.12)$$

$$v_t + \mathbf{V}\cdot\nabla v + (f + ua^{-1}\tan\theta)u = -\frac{(gh)_\theta}{a} - \frac{v}{\tau} + \nu\nabla^2 v, \quad (2.13)$$

$$h_t + \nabla\cdot\mathbf{V}(h - h_B) = \nu\nabla^2 h, \quad (2.14)$$

where ∇ is the horizontal divergence operator, $h = H + \eta$ and h_B is the height of any surface topography (used in Section 5g only). Weak dissipative terms and a weak time filter are added for computational control. The Newtonian term is added to generate or maintain particular zonal flow velocities $u_J(\theta)$ against an equilibrating drag on a time scale τ. These equations are solved using a potential enstrophy conserving scheme on a latitude–longitude grid (Sadourney, 1975). Calculations are made for a channel extending from $\theta = 0$ to 40° and $\lambda = -90°$ to +90°; this wide domain buffers the main vortex region ($\theta = 15$ to 25°) from the boundaries. A resolution of $\Delta\theta = 1°$ and $\Delta\lambda = 2°$ was found to be sufficient. Geometric parameters for Jupiter are $a = 71\,400$ km, $\Omega = 1.763 \times 10^{-4}$ s^{-1}, $H = 10$ km and $g_J = 2640$ cm s^{-2}. Only the parameter combination gH is of dynamical significance, so each solution also holds for $g\alpha^{-1}$ and αH, where α is any number. All solutions are shown in a Northern Hemispheric framework.

3. Jovian vortex parameters

a. Cloud level observation

The properties of the GRS at cloud level are well-known (e.g., Mitchell *et al.*, 1981): it is a singular vortex of great age; it extends (at 21°S) over 12° of latitude and 25° of longitude; at its edge, winds exceed 100 m s^{-1} both zonally and meridionally; it drifts slowly westward (at present) at speeds of 1 to 5 m s^{-1} relative to the System III reference frame (the rotation of the magnetosphere).

The Large Ovals are widely spaced, noncolliding, multiple vortices (3 or 4 in number, at 35°S) that have existed in variable form since 1939. Their winds also reach 100 m s^{-1} at cloud level and they drift eastward at 5 m s^{-1}, relative to System III. The Small Ovals (about 15 in number at 45°S) have a similar drift but a more uncertain form and history.

The vortices of these three sets differ in number, size, history and motion, but they do have similar shapes and spin: all are steep anticyclonic vortices centered on anticyclonic shear zones. A complete theory for these objects should explain this anticyclonic preference, as well as the origin, longevity, form, drift, scale, uniqueness or multiplicity, localization and relationship to the rest of the global circulation.

b. The U scale

The anticyclonic shear zones in which the GRS, Large Ovals and Small Ovals lie are 6–8° wide and bounded by velocity extrema of (−75, 60), (−30, 35) and (0, 40) m s^{-1}, respectively. The location of the vortices at latitudes where u_y^0 is a maximum suggests that they have more of a barotropic than baroclinic energy supply. The barotropic instability criterion for the SW model requires that

$$B = \beta - u_{yy} + \frac{u}{L_R^2} \quad (3.1)$$

change sign for instability. On the largest scales ($\hat{s} \ll 1$), the last term in Eq. (3.1)—the divergence term—dominates the criterion. Application of (3.1) indicates that the cloud-level winds should be highly unstable for almost any reasonable value or variation in $L_R(\theta)$.

However, the fact that the zonal currents do not appear to be particularly unstable implies that they

must, like the ocean currents, have a significant and stabilizing vertical variation—probably an exponential decay with depth. As the SW model represents only the vertically averaged winds, we must assume that they have an amplitude of about one-third the cloud-level values,[11] to avoid excessive barotropic instability. Such velocity levels are used in the scale analysis and numerical solutions.

c. The L_R scale

The primary arbitrary parameter of the SW model is the deformation radius. If we take the most prolific waves to be the best measure of this scale, then $L_R \simeq 1500$ km. The definition $L_R = \sqrt{gH}/f$ produces such values when, for example, $g = g_J/10$ and $H = 10$ km or $g = g_J/100$ and $H = 100$ km. So, unless the atmosphere is both very deep and very stable, this value of L_R is reasonable. The associated long-wave propagation speed $c_\beta = -\beta L_R^2$ equals -10 m s^{-1}. If L_R were larger, c_β would be larger and vortices would propagate at speeds greater than 10 m s^{-1}. As such propagation speeds are not observed, we regard 1500 km as the upper limit for L_R.

It should be noted that for a given value of g and H, L_R can vary considerably with latitude for a vortex as large as the GRS because of the variation in f. Such variations are absent in the β-plane analysis but can be very influential in the spherical case. Thus, in some solutions we allow g to vary as $\sin^2\theta$ to make L_R constant and compare with the β-plane results. In reality, the deformation parameter could vary substantially with latitude and height—as it does for Earth's atmosphere and oceans.

The above choice for L_R is consistent with the planetary view of the global circulation (Williams, 1978, 1979a) in which small baroclinic eddies drive the jets via planetary wave propagation. If, on the other hand, we assume that the medium or large eddies are a better measure of L_R, then we are left without an explanation of the (ageostrophic) small waves and turbulence and without a consistent view of the global circulation.

d. The L scale

The limitations of scale analysis make it impossible to apply the IG theory directly to the Jovian eddies. For the GRS, for example, it is not clear whether the length scale L should be based on the latitudinal radius of 6000 km or on the longitudinal diameter of 26 000 km. The choice can lead to vastly different conclusions.

To illustrate the problem in detail, Table 2 lists the basic SW parameters for three values of L and U, chosen to represent the range of measures of the Jovian eddies and lying nominally in each of the three basic dynamical regimes.

TABLE 2. The basic dimensional and nondimensional dynamical parameters (and the nonlinear factors) for three distinct scales of vortex, located at the latitudes of the major coherent eddy forms on Jupiter—the GRS, Large Ovals and Small Ovals. The observed vortex propagation speed c_{OBS} refers to the drift of these objects relative to System III, where $L_R = 1500$ km, $c_\beta = -\beta L_R^2$, $\hat{\epsilon} = U/Lf_0$, $\hat{\beta} = \beta L/f_0$, $\hat{s} = L_R^2/L^2$, $E = \hat{\epsilon}/\hat{\beta}^2$ and $S = \hat{s}/\hat{\beta}$.

	Big vortex	Medium vortex	Small vortex	Units
L	18 000.	6000.	2000.	km
U	50.	30.	10.	m s^{-1}
f_0	1.3×10^{-4}	2.0×10^{-4}	2.5×10^{-4}	s^{-1}
β	4.6×10^{-9}	4.0×10^{-9}	3.5×10^{-9}	km^{-1} s^{-1}
θ_0	−21°	−35°	−45°	deg
c_{OBS}	−3.	+5.	+8.	m s^{-1}
c_β	−10.	−9.	−8.	m s^{-1}
$\hat{\epsilon}$	0.02	0.02	0.02	
$\hat{\beta}$	0.60	0.12	0.03	
$\hat{s}$	0.01	0.06	0.60	
E	0.05	2.0	25.	
S	0.01	0.5	20.	
$\hat{\epsilon}/\hat{\beta}$	0.3	0.2	0.7	
$\hat{\epsilon}/\hat{s}$	3.0	0.4	0.04	
$\hat{\epsilon}/\hat{\beta}\hat{s}$	5.0	3.0	1.0	
Balance	PG	IG	QG	

e. The dynamical regimes

If we interpret L in Table 2 as the longitudinal diameter of an eddy, then the GRS could be a big vortex and obey PG dynamics. But if we interpret L as the latitudinal radius, the GRS could be a medium IG vortex. Similarly, the Large Ovals could be either IG or QG vortices but the Small Ovals appear to be inescapably of QG form.

For the GRS to exist as a PG vortex, it must be forced by a source of divergence such as a topographic or thermal anomaly in the lower atmosphere. We explore this alternative view of the GRS in Section 5g. Numerical solutions can be used to overcome the vagueness of scale analysis and reveal in which regimes the various vortices lie. These solutions are dealt with in the next two sections.

4. Evolution of monopole IG eddies in shear flows

To see how a solitary IG vortex might behave in the shear zones[12] of Jupiter's atmosphere, we solve the IG equation (2.9) using the parameter values of a medium-sized Jovian vortex ($E = 2$, $S = 0.5$, $U = 30$ m

[11] Similar problems and assumptions arise when the SW model is used for studies of Earth's atmosphere and oceans.

[12] The behavior of IG vortices in uniform flow for ocean parameters has been discussed elsewhere (Matsuura and Yamagata, 1982).

s^{-1}, $L = 6000$ km, $L_R = 1500$ km)—see Table 2. Jovian vortices and mean flows seem to have shears of comparable strength, with divergence effects preventing barotropic instability at these scales. The sign of the vortex and shear are varied to examine different configurations. Gaussian forms of vortex are used to ensure full nonlinearity and generality and collisions are used as an extreme test of stability.

The solutions are shown in a Northern Hemispheric framework, with the (X, y) coordinates propagating westward at the long-wave speed (-9 m s^{-1}). At $y = 1$, the dimensional u and y have values of 30 m s^{-1} and 6000 km.

a. Anticyclonic vortex in anticyclonic shear (A:A)

An initial condition of the form

$$\eta = +1.0e^{-r^2} - 0.5y^2 \tag{4.1}$$

creates a solitary anticyclonic Gaussian vortex in a uniform anticyclonic shear, where $r = (X^2 + y^2)^{1/2}$. The streamfunction, history plot and spectrum describe

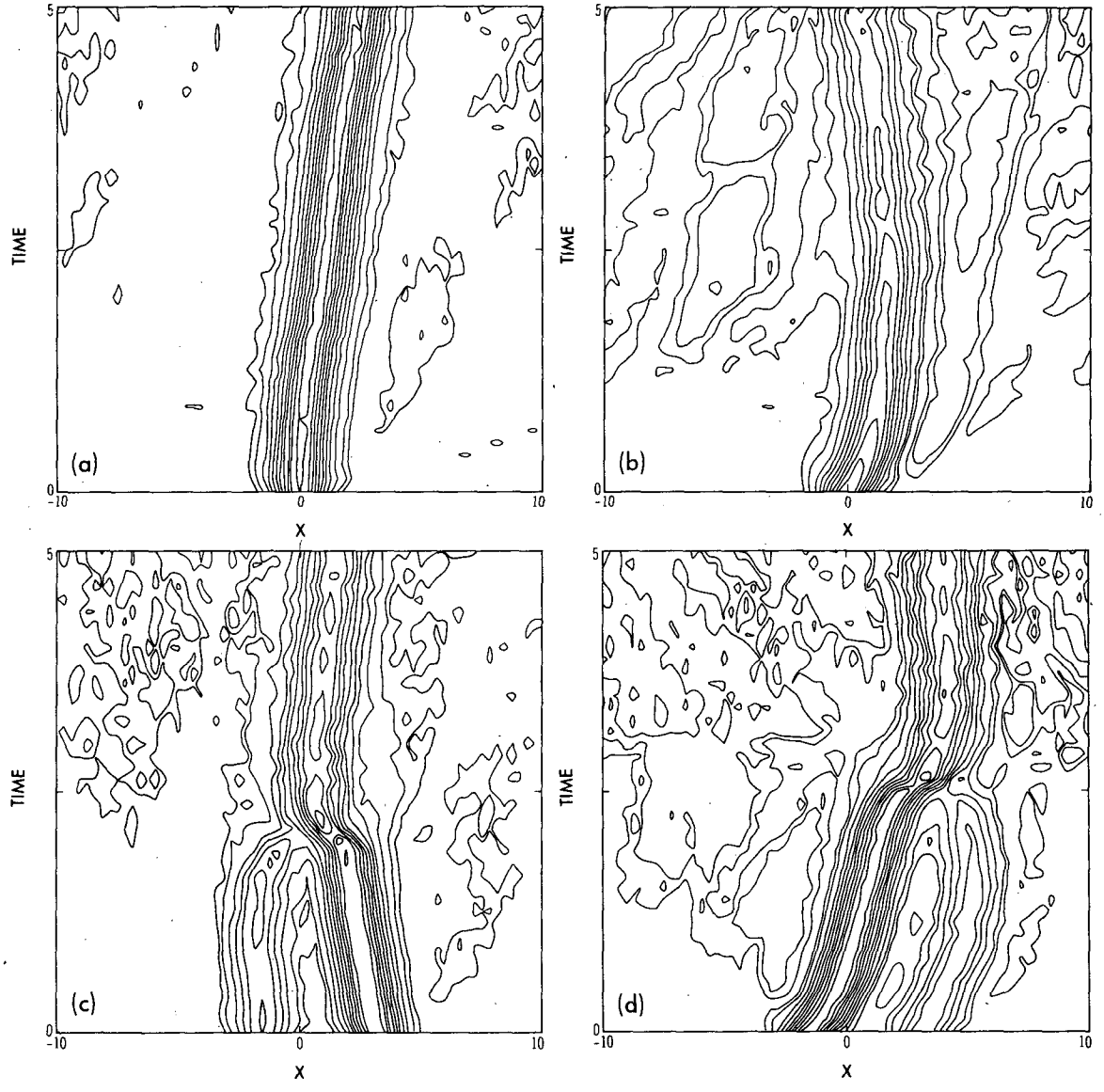

FIG. 1. History plots (time–longitude) of the free surface variable $\eta(X, T)$ at $y = 0$ for the four basic solutions to the IG equation (2.9). (a) (A:A). Anticyclonic vortex in anticyclonic shear; (b) (C:C). Cyclonic vortex in cyclonic shear; (c) (A + A:A). Two colliding anticyclonic vortices in anticyclonic shear; (d) (C + C:C). Two colliding cyclonic vortices in cyclonic shear. The contour interval in (a), (b) is 0.1 plus the ±0.05 values and in (c), (d) it is 0.2 plus the ±0.1 values; no 0.0 values are shown. Domain propagates westward at the long-wave speed. Time is nondimensional; $T = 1$ corresponds to 64 days.

the evolution of this vortex over a time interval $\Delta T = 5$ (Figs. 1a, 2a and 3). The real time, $\Delta T/(f_0\hat{s}\hat{\beta}^2)$, extends to 320 days.

The vortex remains at its original latitude—where $u^0(y) = 0$—but drifts eastward relative to the moving frame due to the meridional asymmetry of the $y\eta_x$ term in Eq. (2.9); see Fig. 1a. Wave propagation creates secondary disturbances to the south, even though a critical layer exists at $y = -0.25$; this occurs because the vortex extends beyond this latitude. A turning point at $y = +0.25$ eliminates waves to the north of the vortex. Except for determining the position of the critical layer and the turning point and producing a slight longitudinal stretching, the meridional shear has little effect on the vortex behavior—mainly because $SE^{-1} \gg |u^0|$ near the vortex. Unlike the QG soliton, the vortex can exist without shear.

This vortex is said to be *robust*, or strongly stable, as its identity and integrity are easily maintained by a balance between the dispersion and nonlinear steepening terms. Little energy disperses at any wavenumber (Fig. 2a). The durability also depends to some extent on the values of E and S, factors whose relative magnitude control the slow time scale. When $E = 0.4$, $S = 0.6$, for example, a vortex disperses more rapidly.

b. *Cyclonic vortex in cyclonic shear (C:C)*

The initial condition

$$\eta = -1.0e^{-r^2} + 0.5y^2 \tag{4.2}$$

creates a cyclonic vortex in a cyclonic shear. The eddy initially moves northward (due to self-induction) and relatively eastward (due mainly to the $ES^{-1}\eta\eta_x$ term), before settling at the long-wave speed as its decay progresses (Figs. 1b and 4). The weak eddies emitted from the original vortex continue to show a weak but systematic relative-eastward propagation because their lateral scale is small (Fig. 1b).

The collapse of the vortex occurs at all scales (Fig. 2b), but mainly on its southern side because $S + Eu^0 > 0$ there. This prevents a balance between the dispersion and the nonlinear steepening. A critical layer at $y = +0.25$ prevents wave propagation and collapse on the northern side (where $S + Eu^0 \leq 0$). An example

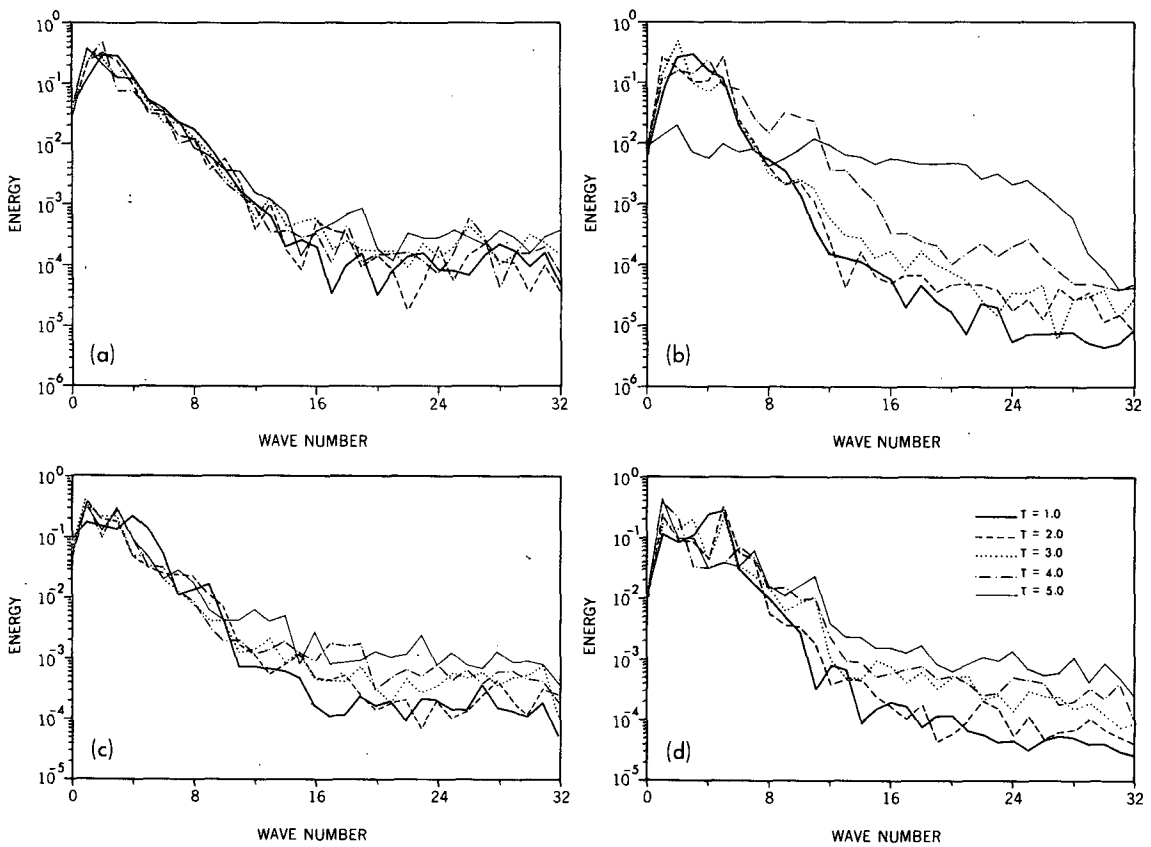

FIG. 2. As in Fig. 1 (a)–(d), but for kinetic energy spectra in terms of the zonal wavenumber, with mean flow component subtracted.

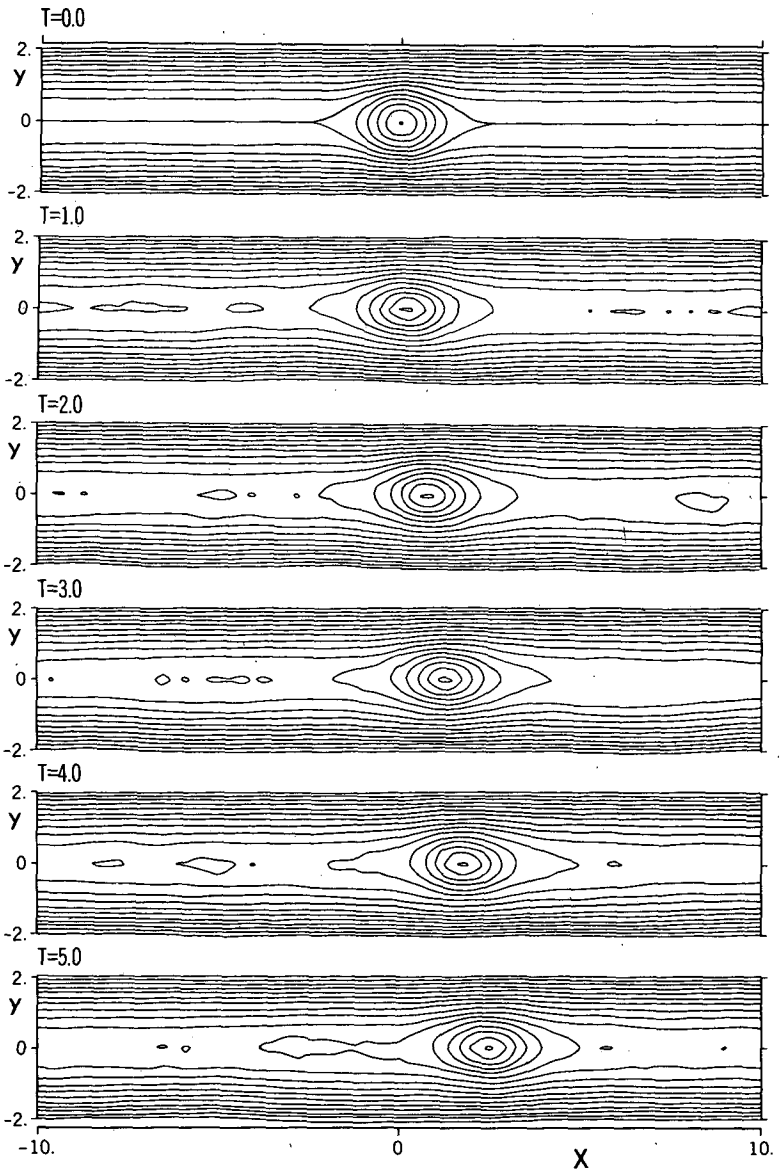

FIG. 3. IG Solution (A:A). Evolution of the free surface variable $\eta(X, y, T)$ for an anticyclonic Gaussian vortex in an anticyclonic shear. The contour interval is 0.2 and the time interval $\Delta T = 1.0$ corresponds to 64 days. Domain propagates westward at the long-wave speed. Only the central part $y = \pm 2$ of a computational domain of $y = \pm 10$ is shown. At $y = \pm 2$, the dimensional u, y values are ± 60 m s^{-1} and $\pm 12\,000$ km.

of a robust cyclonic vortex in an $S + Eu^0 = 0$ flow is given by Matsuura and Yamagata (1982).

c. Collision of two anticyclonic vortices in anticyclonic shear (A + A:A)

The initial condition

$$\eta = 1.0 \exp - [(X + 1.56)^2 + y^2] + 2.0 \exp\{- [(X - 3.13)^2 + y^2]\} - 0.5y^2 \quad (4.3)$$

creates two anticyclonic vortices traveling westward at different speeds (due to their different intensities) in an anticyclonic shear zone (Figs. 1c and 5). The stronger eddy moves more rapidly, catching up with the weaker one and absorbing it. (Vortices of equal intensity and size travel at the same speed and never collide.) The collision changes the eddy propagation from relative-westward to relative-eastward (Fig. 1c) and transfers energy to the larger scale (Fig. 2c; cf. curves for $T = 1$ and $T = 3$).

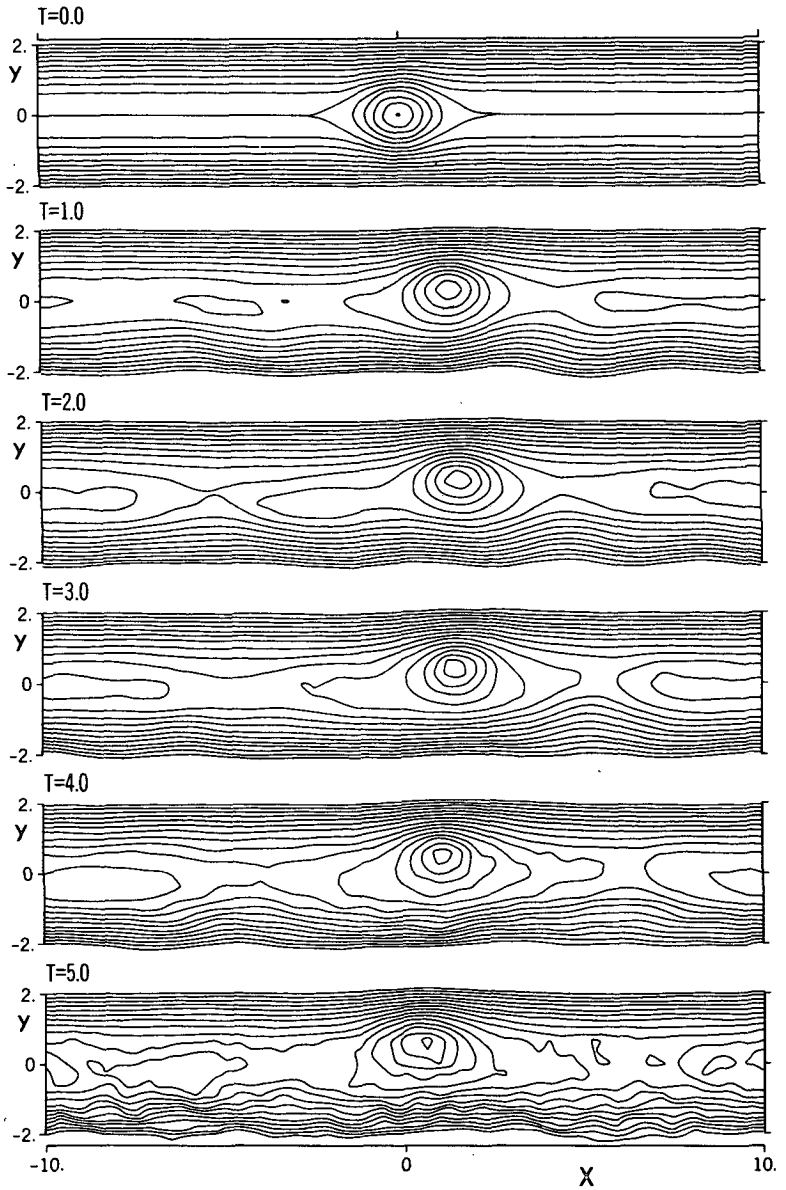

FIG. 4. As in Fig. 3, but for IG Solution (C:C). Evolution of the free surface variable $\eta(X, y, T)$ for a cyclonic Gaussian vortex in a cyclonic shear.

The coalescing of eddies is normal behavior for two-dimensional fluids both for deterministic (Winant and Browand, 1974) and statistical (Batchelor, 1959, p. 187) systems. Merging also occurs for quasi-geostrophic motions, for a singular vortex (cf. Ingersoll and Cuong, 1981) and for turbulence (Rhines, 1977). The nonlinear advection Jacobian controls the coalescence in all these systems. In IG dynamics, however, the Jacobian is only active during collisions. The Jacobian term of (2.9) is zero for a circular vortex and becomes significant only when strong deviations from circular motion occur—such as during collisions. Only in the absence of collisions do the vortices obey a form of one-dimensional Korteweg-deVries (KdV) equation. Soliton behavior, in which vortices pass through each other with only a phase shift as a remnant of collision, is abnormal and peculiar to motions obeying the pure KdV equation (cf. Miles, 1980); however, recent studies have shown that certain QG modons also exhibit soliton behavior (McWilliams and Zabusky, 1982).

We cannot argue that a large IG solitary vortex can sustain itself by absorbing smaller IG vortices, because at some point we would have to explain how a smaller IG eddy sustains itself by interaction with the QG scale

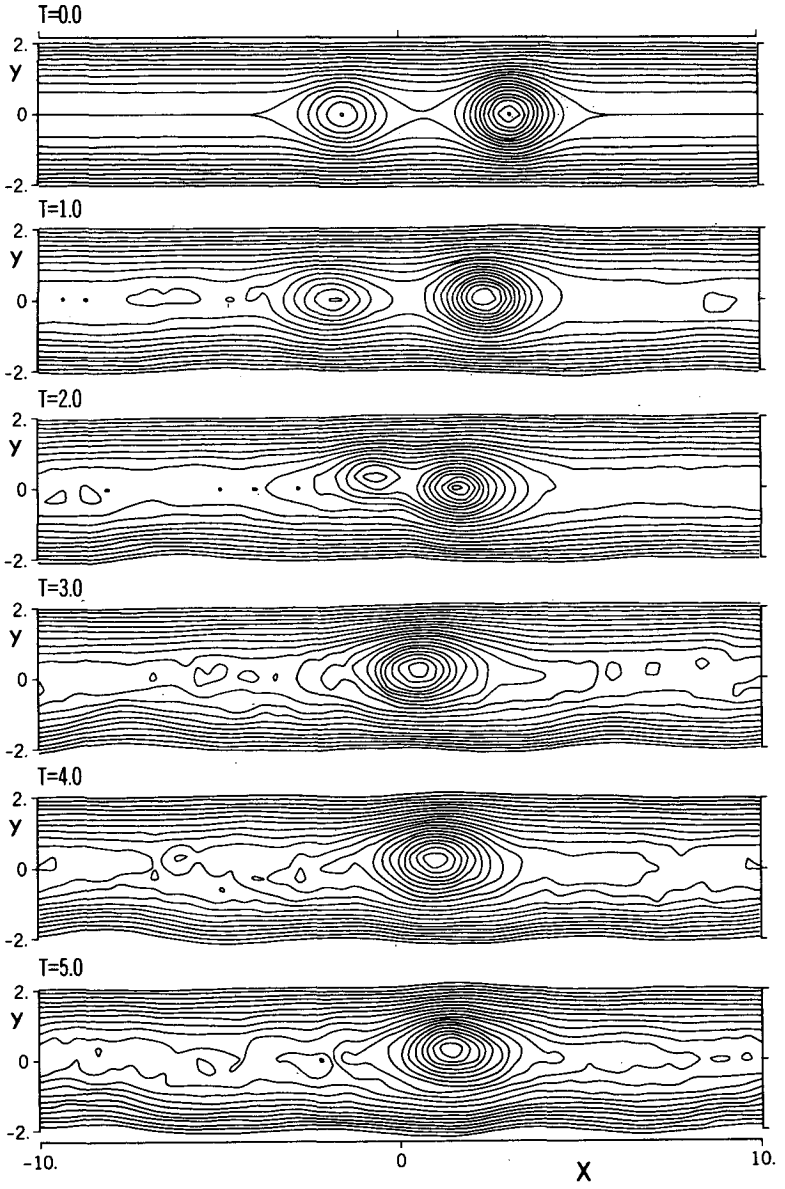

FIG. 5. As in Fig. 3, but for IG Solution (A + A:A). Evolution of the free surface variable $\eta(X, y, T)$ for two colliding anticyclonic Gaussian vortices in an anticyclonic shear.

motions and, as we shall see in Section 5, such interactions tend to disperse the vortex.

d. Collision of two cyclonic vortices in cyclonic shear (C + C:C)

The initial condition

$$\eta = -2.0 \exp - [(X + 1.56)^2 + y^2] - 1.0 \exp\{- [(X - 3.13)^2 + y^2]\} + 0.5y^2, \quad (4.4)$$

produces two cyclonic vortices of unequal intensity traveling relatively eastward and slightly northward in a cyclonic shear zone (Figs. 2d and 6). They coalesce into a larger vortex that has almost no relative motion and which disperses in the manner of the simple cyclonic vortex in Section 4b. Some of the amplitude loss seen in Fig. 1d comes from the northward displacement of the vortices.

Comparing the dispersion rates of the single and colliding cyclonic vortices, Figs. 2b and 2d, suggest that the normal collapse of a cyclonic vortex is slightly delayed by the absorption of a smaller vortex.

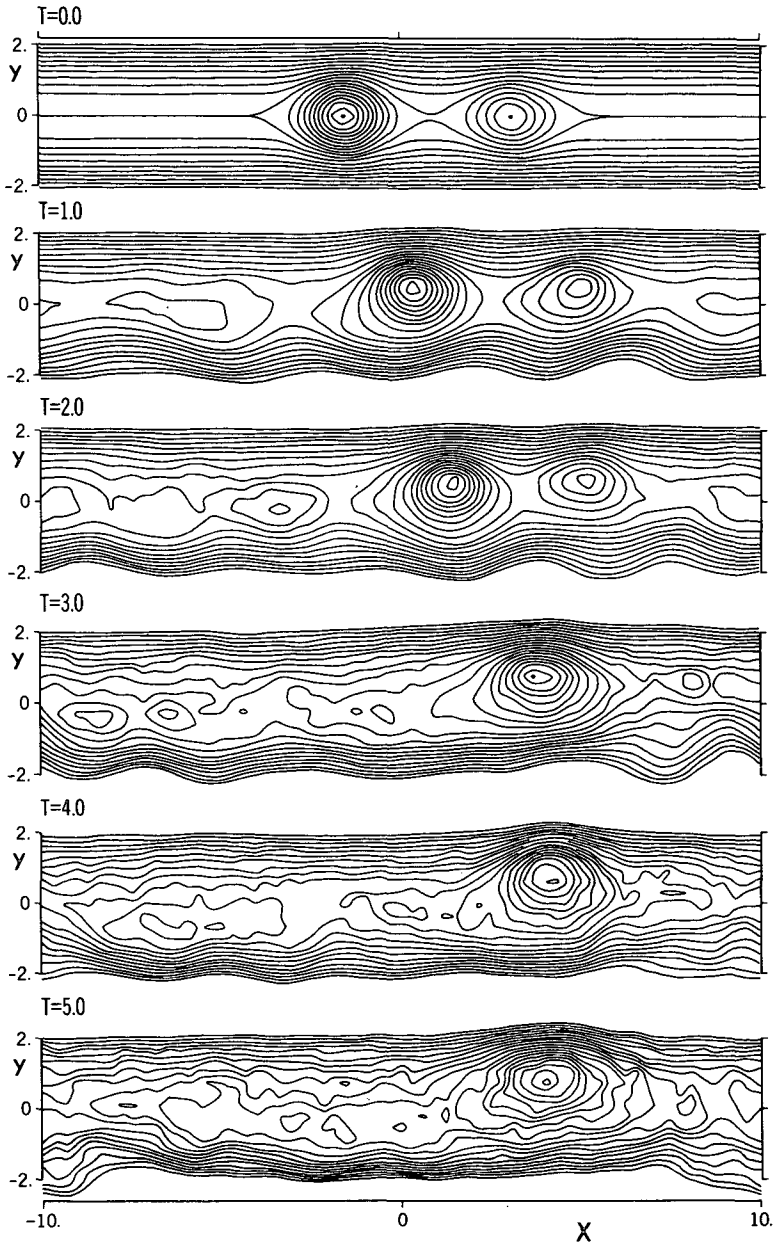

FIG. 6. As in Fig. 3, but for IG Solution (C + C:C). Evolution of the free surface variable $\eta(X, y, T)$ for two colliding cyclonic Gaussian vortices in a cyclonic shear.

e. Anticyclonic disturbance in cyclonic shear (A:C)

To examine the stability of anticyclonic eddies further, we place such an eddy in an opposing, cyclonic shear via the initial condition

$$\eta = 1.0e^{-r^2} + 0.5y^2. \tag{4.5}$$

This produces a saddle-shaped disturbance which, after some initial adjustment, remains intact for the rest of the calculation (Fig. 7). The inverse configuration, a cyclonic eddy in an anticyclonic shear, evaporates quickly (not shown).

f. Anticyclonic vortex in multi-jet flow (A:mA)

To see what happens when the environmental shear zone is only as wide as the vortex, we place an anticyclonic vortex in the central anticyclonic region of a multi-jet flow (Fig. 8) using the initial condition

$$\eta = 1.0e^{-r^2} + \cos y - 1.0. \tag{4.6}$$

This configuration eliminates the boundary problems associated with computing for narrow shear zones in narrow channels.

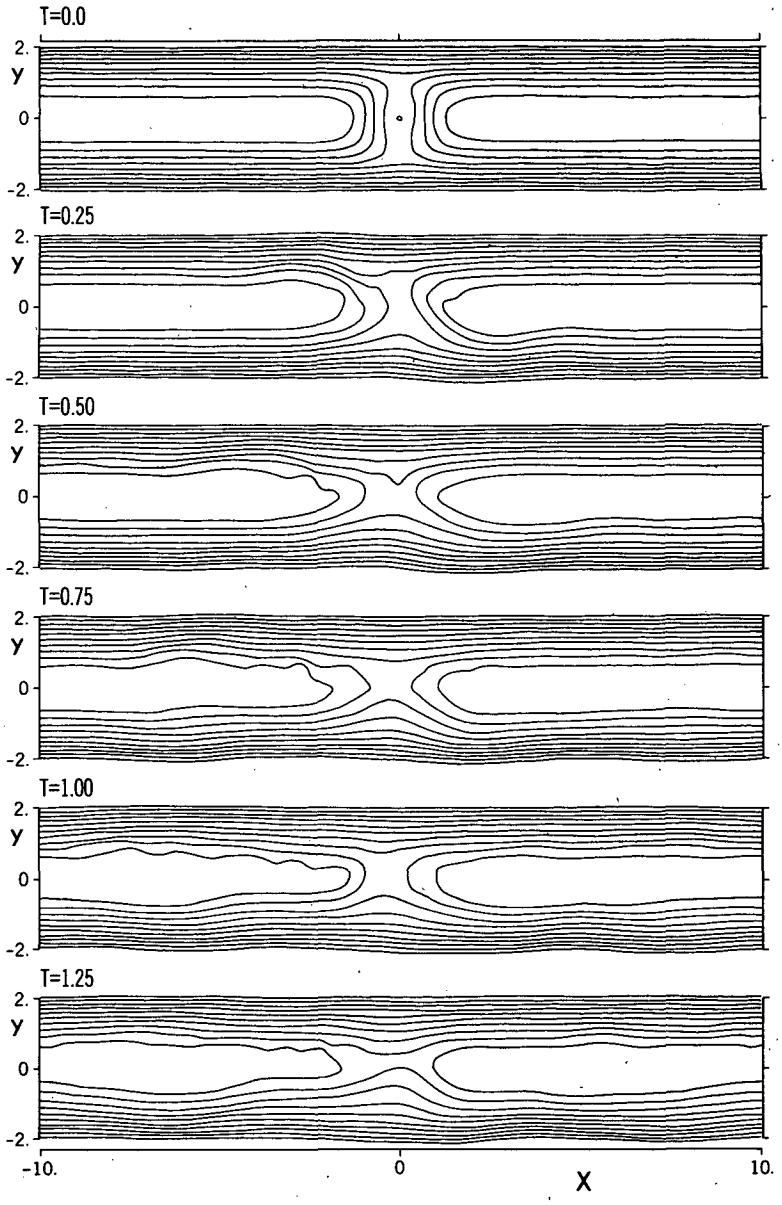

FIG. 7. As in Fig. 3, but for IG Solution (A:C). Evolution of the free surface variable $\eta(X, y, T)$ for an anticyclonic Gaussian vortex in a cyclonic shear.

The vortex evolves much like the basic case in Section 4a, traveling relatively eastward at its original latitude and remaining robust. This similarity is to be expected, given the weak impact of any shear on an IG vortex. Differences occur with the secondary eddies: propagation northward and southward is limited by multiple turning points and critical layers [at $y \approx n\pi + (-1)^{n+1}\, 0.25$]. The weak waves south of the vortex propagate relatively westward since the vortex initially extends into the region where $S + Eu^0 < 0$. Small disturbances are observable in the various zones where $u^0 = 0$ because the basic η is small there.

5. Origin and evolution of Jovian (SW) vortices

The vortices of Section 4 are constrained, by virtue of our use of the restricted equation (2.9), to be of a purely IG form. We now examine whether IG vortices can exist (with and without zonal flows) in the more general dynamical and geometrical framework of the full spherical SW equations (2.12)–(2.14). We find that they can, despite the possible presence of dispersive QG modes, and that they resemble the GRS and Large Ovals when Jovian parameters are used.

The behavior of a large anticyclonic vortex on a

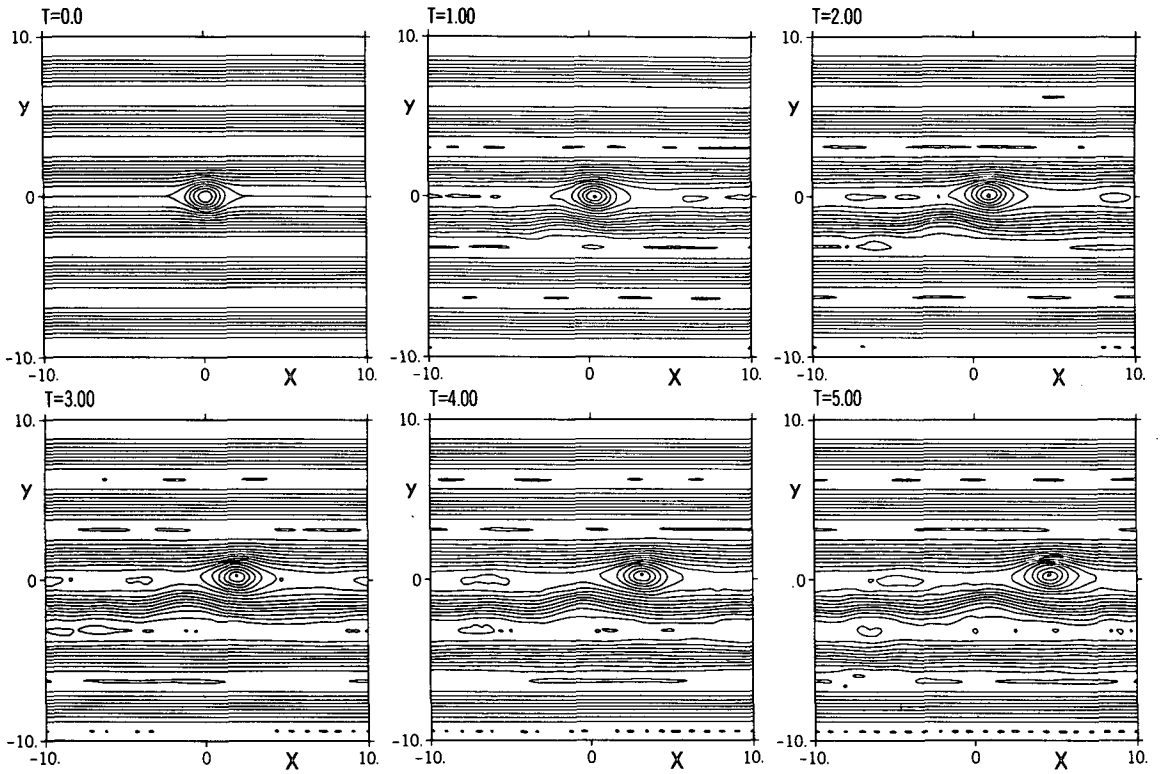

FIG. 8. As in Fig. 3 except whole domain is now shown for IG Solution (A:mA). Evolution of the free surface variable $\eta(X, y, T)$ for an anticyclonic Gaussian vortex placed in the central anticyclonic shear zone of a multiple jet flow.

sphere with Jovian parameters depends mainly on the value of the static-stability parameter g (or L_R). When the stability is high ($g > g_J/5$), the vortices are large and QG, but when the stability is low ($g < g_J/20$) they are small and ageostrophic. When the stability is moderate ($g_J/20 < g < g_J/5$), IG vortices form that retain their identity for a long time and propagate uniformly westward at a speed close to c_β. Vortex stability is marginal for $g_J/10 < g < g_J/5$, but can be enhanced by the presence of a zonal flow or a variable $g(\theta)$. These values of g are obtained for vortices of GRS scale and location and for $H = 10$ km. All vortices are initially stationary and of anticyclonic Gaussian form.[13]

a. Evolution when g = constant ($u^0 = 0$)

A vortex placed at $\theta = 25°$ on a Jovian sphere with $g = g_J/15$ evolves as shown in Fig. 9. The initially stationary vortex sheds a tail as it begins to propagate and to adjust to an IG balance. It travels westward at -10 m s^{-1}, a speed close to the theoretical value of c_β (-7 m s^{-1}) at $\theta = 21°$. Over the 3-year period, the eddy decays because the relatively high static-stability imposed on the equatorial region leads to anomalously strong wave activity in that region.

This vortex differs significantly from those on the IG β-plane: its shape is no longer circular, its axis tilts and it migrates slowly equatorward. These differences are due to the stronger meridional twisting and the significant latitudinal variations in the basic parameters L_R and c_β over the region of this large vortex.

b. Evolution when L_R = constant ($u^0 = 0$)

Eddies on a sphere resemble those on the IG β-plane most closely when they are relatively small. However, large circular vortices can be generated on a sphere, and in low latitudes, by forcing g to vary as $\sin^2\theta$. This makes L_R and c_β (almost) independent of θ. Writing the pressure term as $(gh)_\theta$ in Eq. (2.13) achieves this without violating the consistency of the SW system. If g varies as $(1 + \hat{\beta}yg')$ on the IG β-plane, the terms (ii) and (iv) in (2.9) are modified by factors of $(1 + g')$ and $(1 - \frac{1}{2}g')$ respectively; this implies that the stability is enhanced and the meridional twisting is reduced by such variations. Variations in g are physically unrealistic but are a useful mathematical device for connecting the IG β-plane and spherical analyses.

The evolution of a vortex placed at $\theta = 21°$ in a

[13] Cyclonic vortices disperse within 50 days and will not be presented. A day is 86 400 seconds.

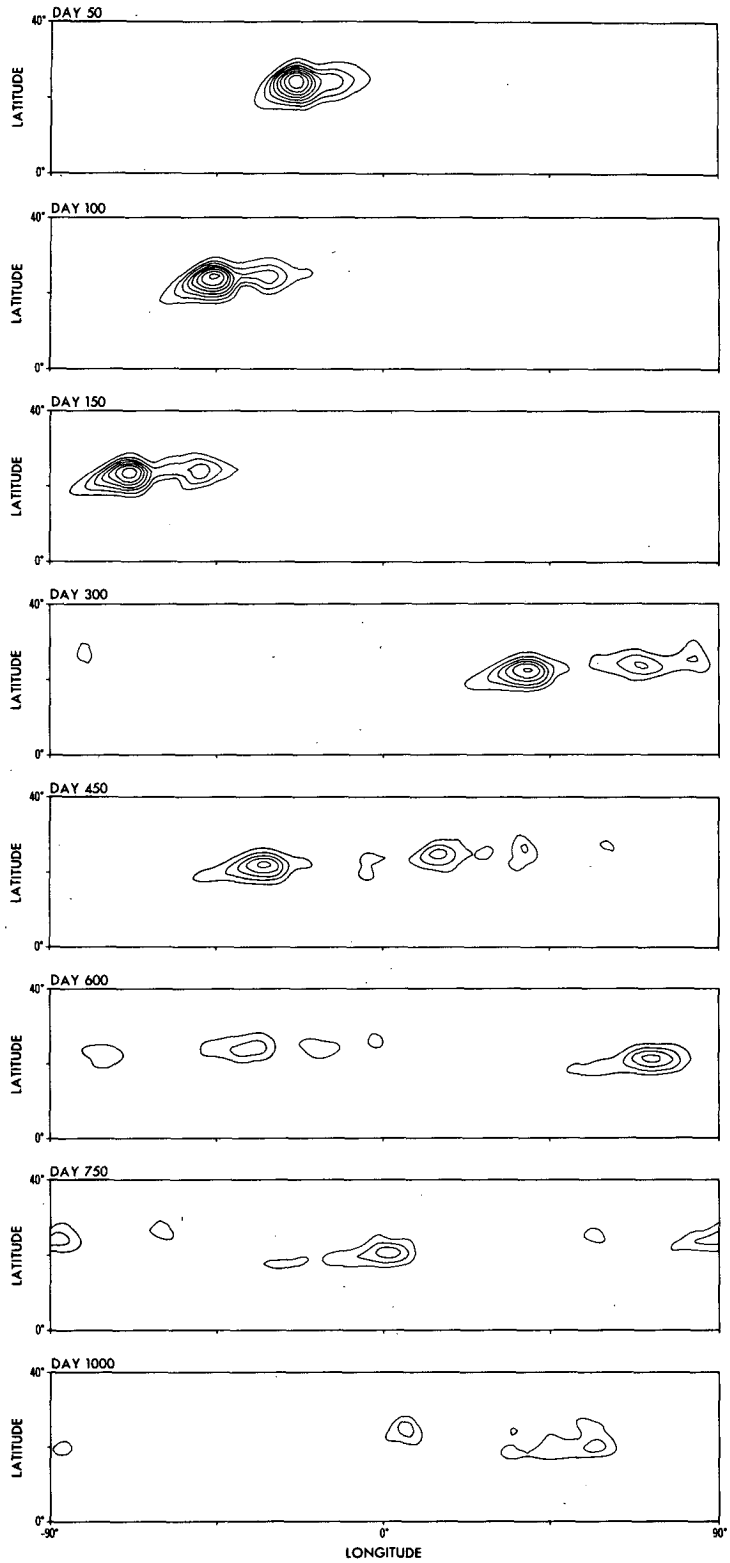

FIG. 9. Solution SW1. Evolution of the free surface variable $\eta(\lambda, \theta)$ for an anticyclonic vortex in a resting fluid, with $g = g_J/15$. Contour interval is 1 km. Initial vortex has a diameter of $\sim 10°$, $U \approx 20$ m s^{-1}, $\theta = 25°$ and $\lambda = 0°$. Jovian parameter values are as in Section 2f, with $\tau = 5 \times 10^7$ s and $\nu = 0.01$ km^2 s^{-1}.

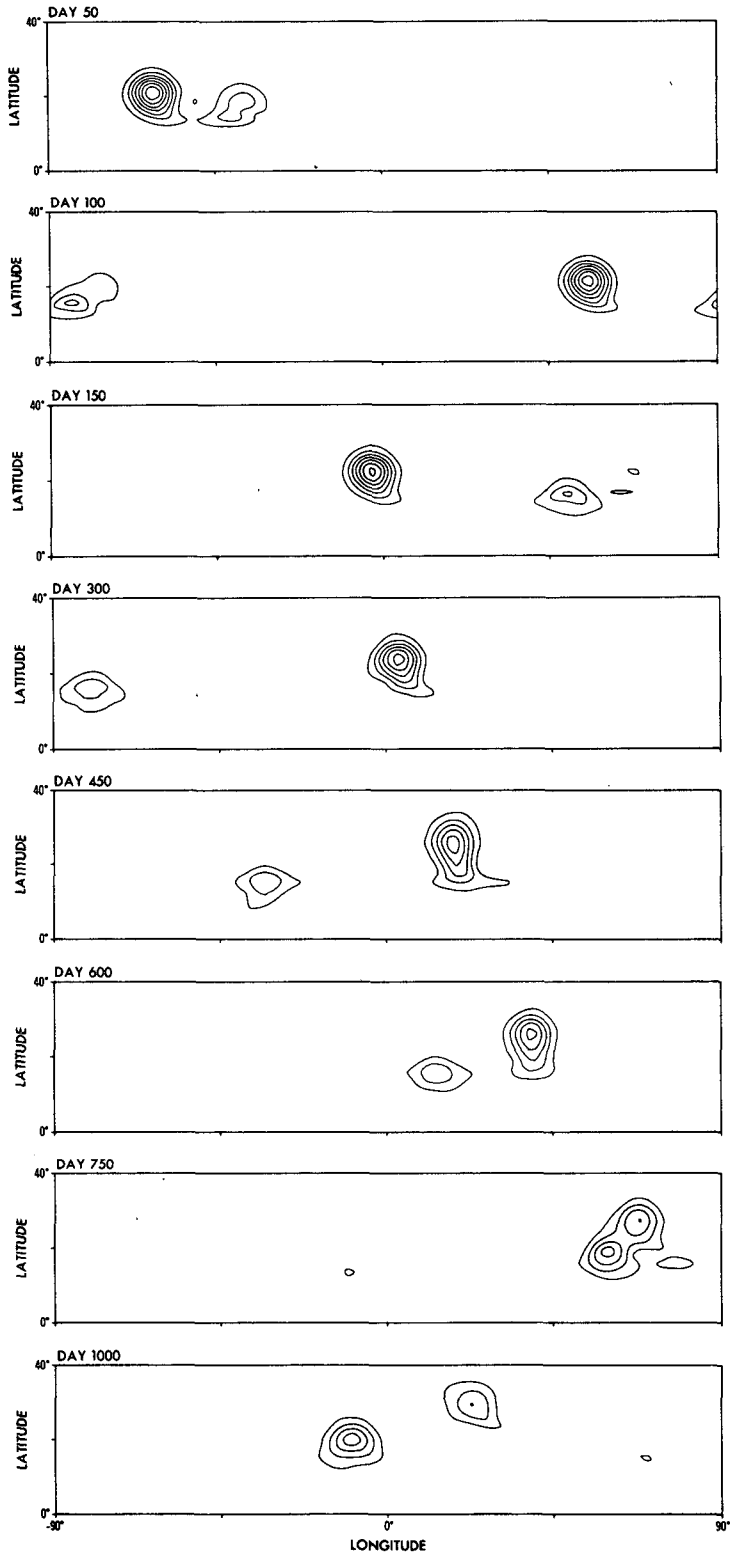

FIG. 10. Solution SW2. Evolution of the free surface variable $\eta(\lambda, \theta)$ for an anticyclonic vortex in a resting fluid with constant L_R; $g = \frac{1}{10}g_J G(\theta)$, $\theta > 5°$. Contour interval is 1 km. Initial vortex has a diameter of $\sim 10°$, $U \approx 20$ m s^{-1}, $\theta = 21°$ and $\lambda = 0°$. Jovian parameter values are as in Section 2f, with $\tau = \infty$ and $\nu = 0.01$ km^2 s^{-1}.

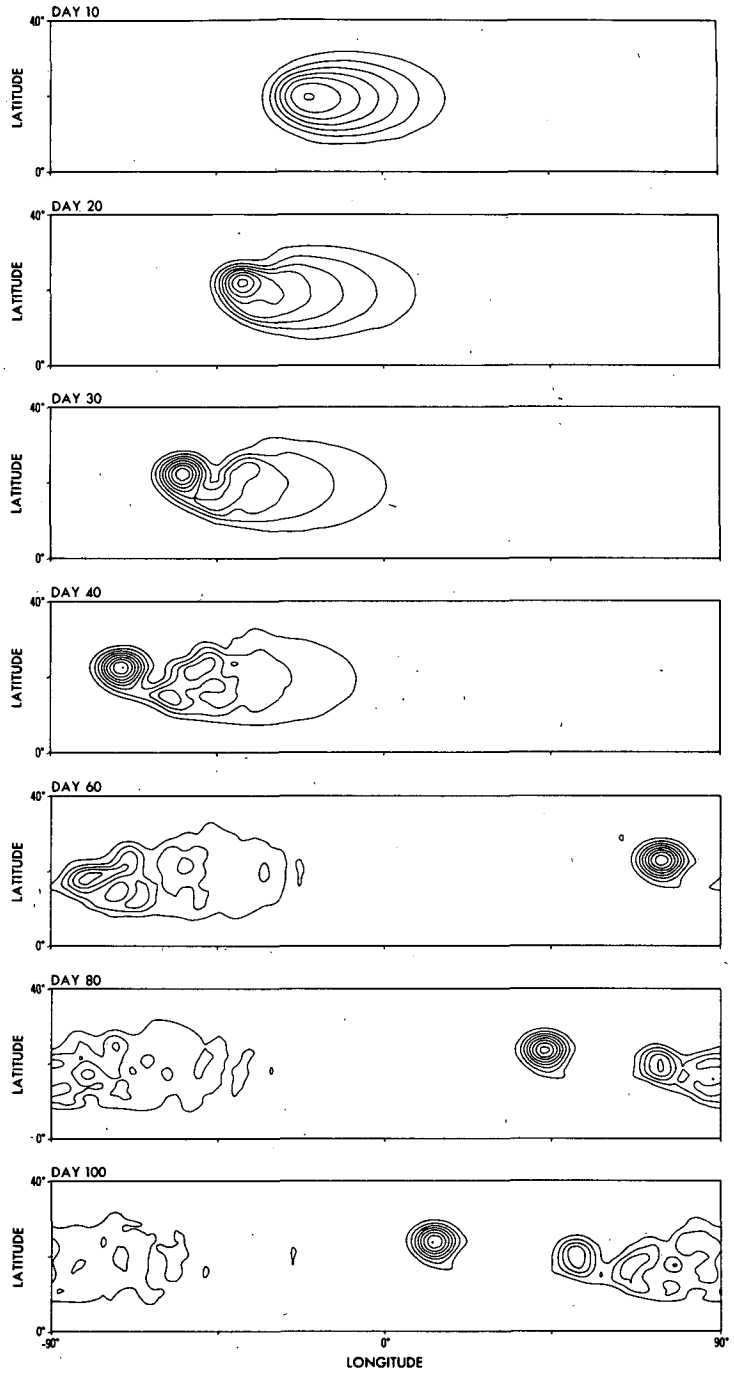

FIG. 11. Solution SW3. Adjustment of an overly large anticyclonic vortex to the preferred IG scale, in a resting fluid with constant L_R; $g = \frac{1}{15} g_J G(\theta)$. Contour interval of $\eta(\lambda, \theta)$ is 2.5 km. Initial vortex has a diameter of ~20°, $U \approx 20$ m s^{-1}, $\theta = 21°$ and $\lambda = 0°$. Jovian parameter values are as in Section 2f, with $\tau = 5 \times 10^7$ s and $\nu = 0.05$ km^2 s^{-1}.

fluid with a constant L_R is shown in Fig. 10, where $g = g^* G(\theta)$, $g^* = g_J/10$ and $G(\theta) = \sin^2\theta/\sin^2 21°$. The eddy still decays due to computational effects, but appears to be substantially more stable than the vortex of the previous solution. The tail shed by the initial adjustment forms an equally stable vortex. The main vortex drifts westward at -12 m s^{-1} ($c_\beta = -10$ m s^{-1} at $\theta = 21°$) and migrates slowly poleward. It eventually catches up with the more slowly moving tail-vortex and transfers much of its energy equatorward into it,

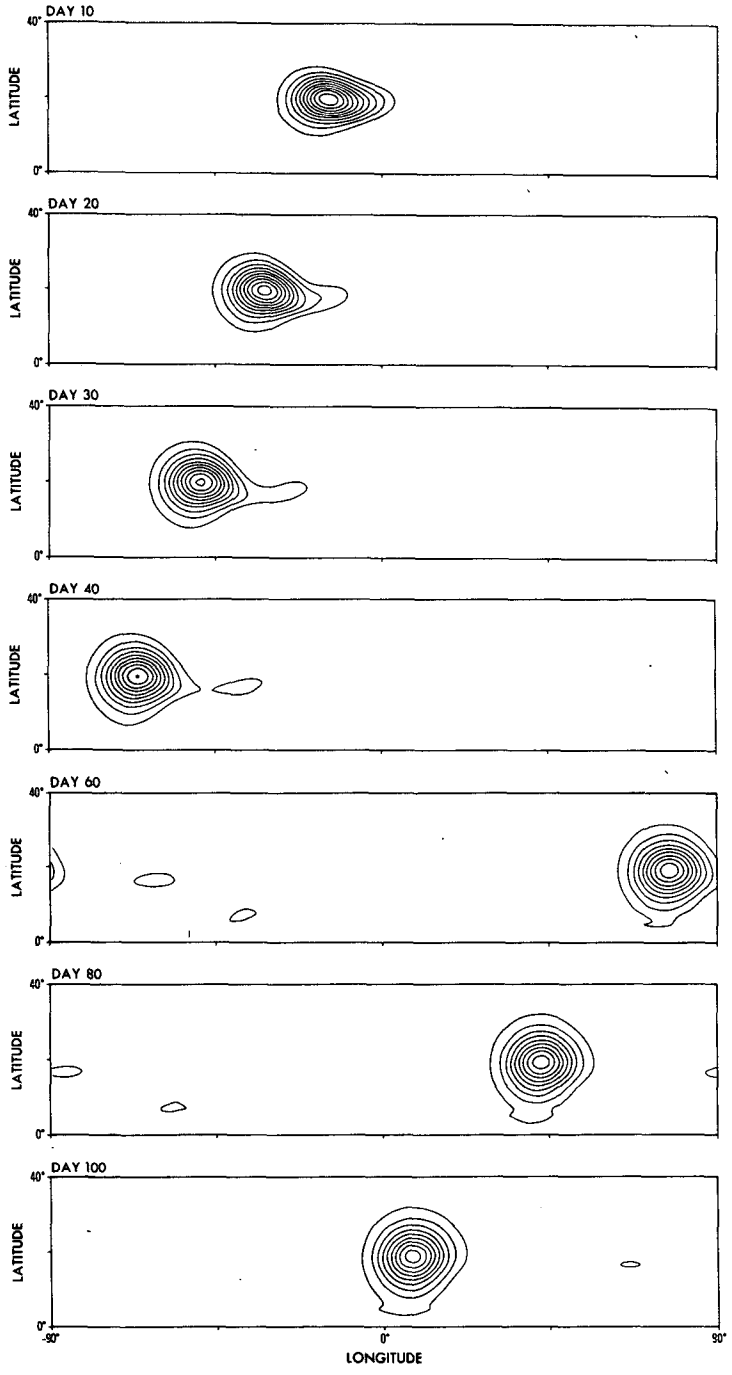

FIG. 12. Solution SW4. Adjustment of an overly small anticyclonic vortex to the preferred IG scale, in a resting fluid with constant L_R; $g = \frac{1}{3} g_J G(\theta)$. Contour interval of $\eta(\lambda, \theta)$ is 0.3 km. Initial vortex has a diameter of $\sim 10°$, $U \approx 20$ m s^{-1}, $\theta = 21°$ and $\lambda = 0°$. Jovian parameter values are as in Section 2f, with $\tau = 5 \times 10^7$ s and $\nu = 0.05$ km^2 s^{-1}.

recreating a strong singular vortex at the original latitude. Such events are unusual, but they illustrate the coalescence mechanism of the IG system. Vortices with the variable g remain stable for $g_J/20 < g^* < g_J/5$.

c. *Preferred scales*

Vortices appear to have a preferred size for a particular value of L_R and adjust their initial form to

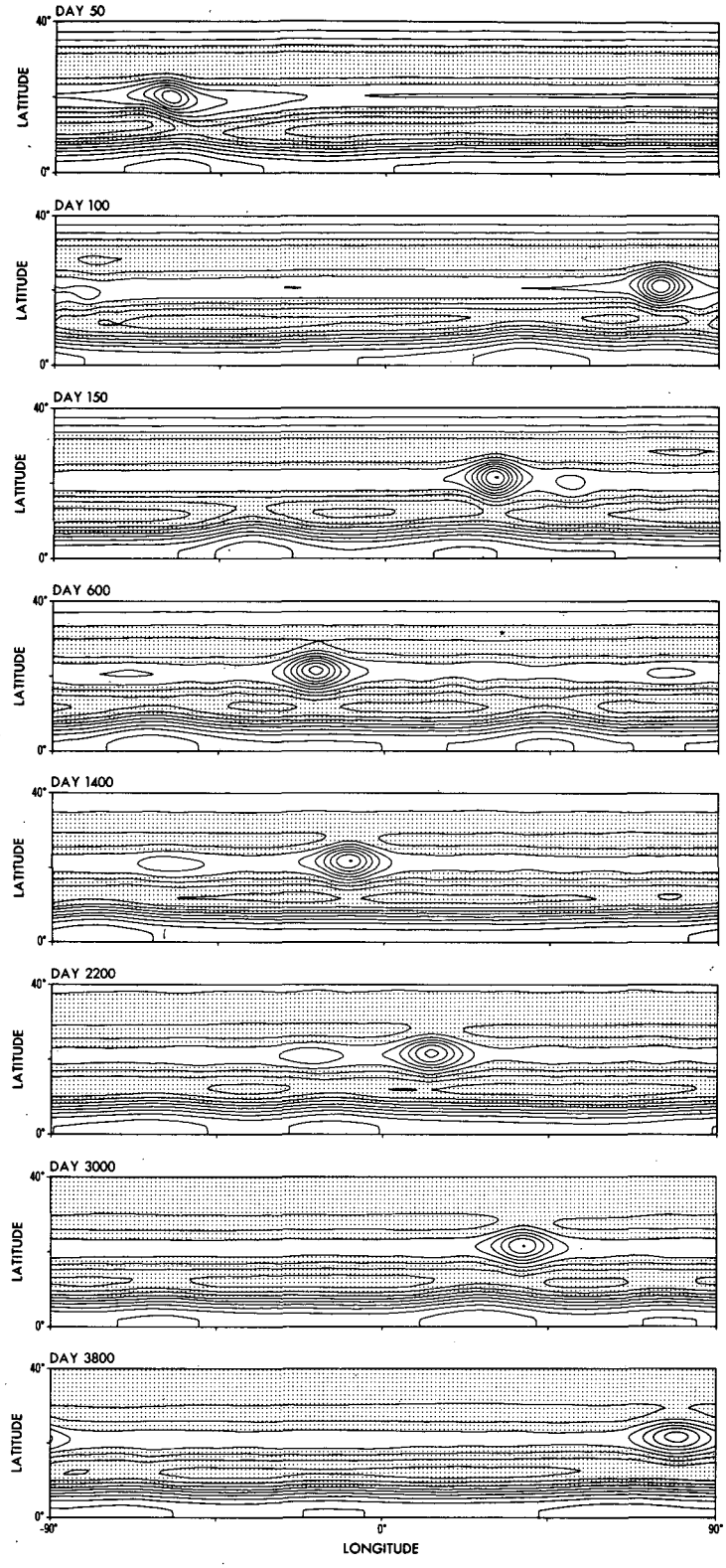

FIG. 13. Solution SW5. Evolution over one decade of the free-surface variable $\eta(\lambda, \theta)$ for an anticyclonic vortex in an anticyclonic shear zone (as profiled in Fig. 16), with $g = g_J/8.5$. Contour interval is 1 km; negative values are shaded. Initial vortex has a diameter of $\sim 10°$, $U \approx 20$ m s^{-1}, $\theta = 21°$ and $\lambda = 0°$. Shear zone has an initial amplitude of +20 m s^{-1} and width of 8° in latitude. Jovian parameter values are as in Section 2f, with $\tau = 5 \times 10^7$ s and $\nu = 0.01$ km^2 s^{-1}.

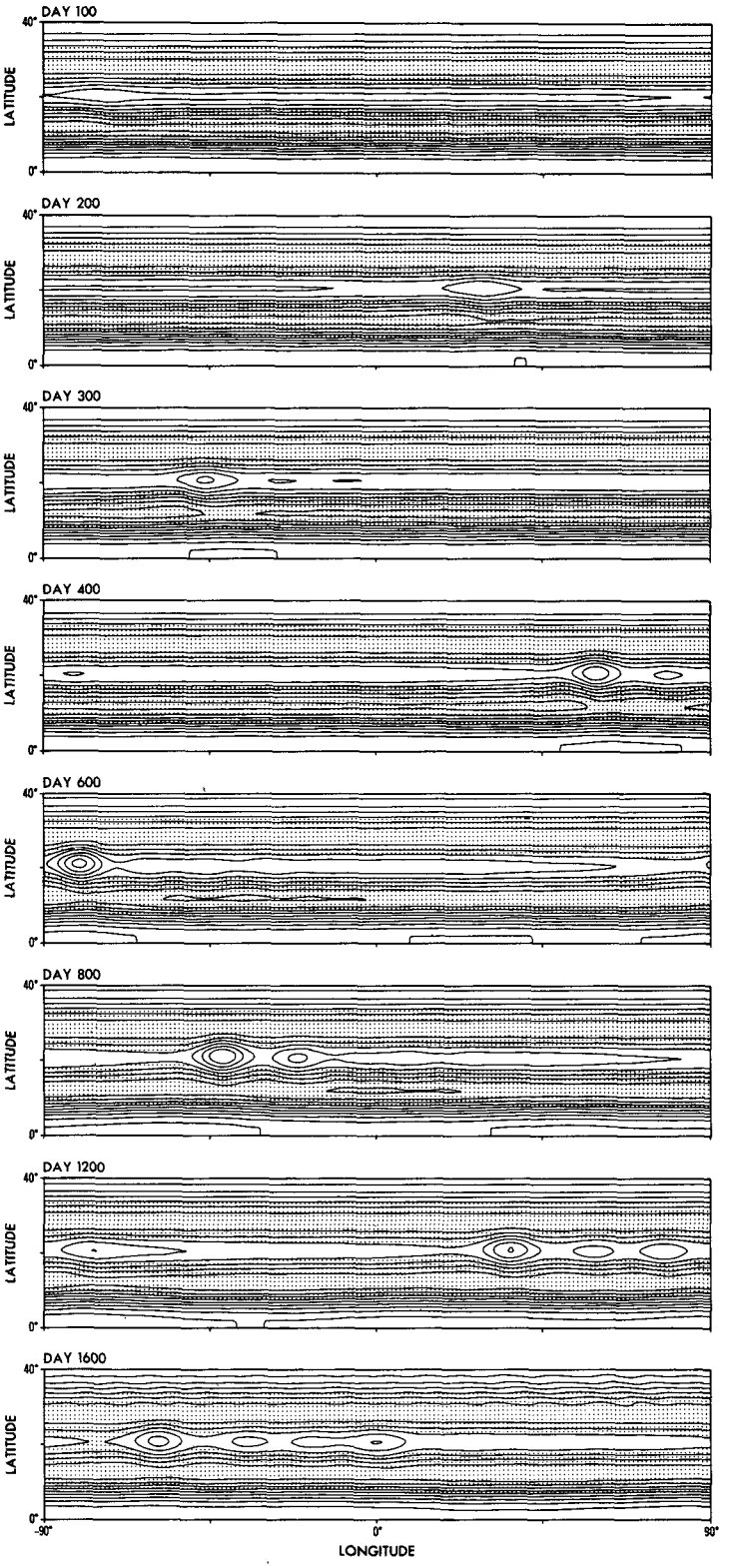

FIG. 14. Solution SW6. Growth of a weak, localized disturbance in a weakly (barotropically) unstable anticyclonic shear zone (as profiled in Fig. 16), with $g = g_J/10$. Contour interval for the free-surface variable $\eta(\lambda, \theta)$ is 1 km; negative values are shaded. Initial disturbance is at $\theta = 21°$ and $\lambda = 0°$. Shear zone has an initial amplitude of +25 m s^{-1} and a width of 8° in latitude. Jovian parameter values are as in Section 2f, with $\tau = 10^7$ s and $\nu = 0.1$ km^2 s^{-1}.

achieve this scale and an IG balance. For example, the overly large eddy in Fig. 11 shrinks to the smaller scale preferred at $g^* = g_J/15$ by shedding a large tail, which in turn condenses into two vortices of the same size as the main eddy. An overly small vortex expands just until it reaches the optimum size for $g^* = g_J/5$ (Fig. 12). (Similar results are obtained with g = constant.) Eddies whose initial size is close to the optimum behave as in Figs. 9 and 10.

d. *Longevity of a GRS-like vortex*

The stability of an anticyclonic vortex, such as the one in Fig. 9, is considerably enhanced when it lies in the anticyclonic shear zone of barotropically stable zonal currents. For the example shown in Fig. 13, only a slight weakening of the vortex and currents occurs over the 10-year period of integration, even though 2×10^5 time steps are involved. The zonal flow enhances the stability of the IG vortex by blocking the development of dispersive QG wave propagation, as discussed in Section 4a. The currents also prevent the latitudinal migration of the vortex. The tendency of a vortex to drift latitudinally (Figs. 9 and 10) and its blocking by zonal currents (Fig. 13) could explain the 90-day latitudinal oscillation of the GRS (see, for example, Hunt and Moore, 1981). The small tail shed during the initial phase is reabsorbed approximately seven years later.

The pattern and scale of the flow in Fig. 13 resemble that of Jupiter's GRS and zonal currents. The flow amplitudes, however, are weaker than the *cloud-level* observations, in anticipation of the vertical variation in the winds. The vertical motion within the IG vortex is upward within the western half and downward in the eastern half, due mainly to the drift to the vortex, i.e., $w \simeq \eta_t$ (Fig. 15). The weakness of the vertical motion ($w < 0.5$ cm s^{-1}) compared to the horizontal motion prevents its being directly observable. There are indirect indications of such upflows for the GRS (R. F. Beebe, personal communication, 1983).

The vortex propagation speed is larger than that of the GRS: -12 m s^{-1} ($=c_\beta$ at $\theta = 21°$) versus -5 m s^{-1} (measured relative to System III). Only smaller IG vortices, with $L_R = 1000$ km and $g = g_J/20$, have drift rates of -5 m s^{-1}. Thus, if *size* (at cloud level) is the best guide to its nature, the GRS may actually be propagating more rapidly westward than estimates relative to System III indicate. If this is so, the reference frame is unsuitable and all Jovian flows may be more easterly (by 5–10 m s^{-1}) than it indicates. Alternatively, in a continuously stratified atmosphere, vertical variations in L_R, etc. may yield IG vortices that drift more slowly than their SW counterparts.

e. *Genesis of a GRS-like vortex*

While the above solutions, especially the one in Fig. 13, hint at why the GRS is such a stable eddy, they do not tell us how the vortex originated. There are many possible ways, but only those that relate to existing conditions can be tested scientifically. We examine the simplest possibility, i.e., that the vortex was created by a weak barotropic instability and is also maintained by such against weak dissipation effects. (Strong instabilities are excluded as they tend to create multiple vortices.) To create a single vortex with a strong internal balance using a weak external source acting over a long time is computationally difficult.

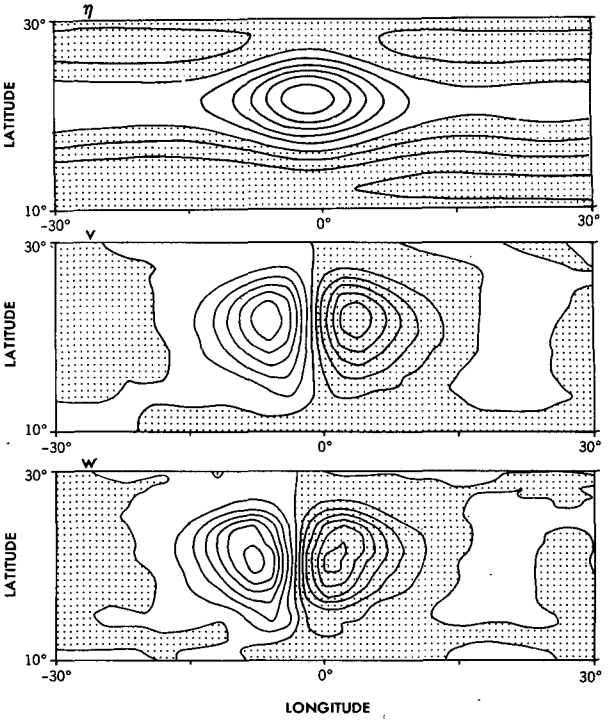

FIG. 15. Solution SW5 detailed at Day 1800. Closeup of the free-surface, meridional velocity and vertical velocity (at $z = H$) variables for the GRS-like anticyclonic vortex in the anticyclonic shear zone of Fig. 13. Contour intervals are 1 km, 2.5 m s^{-1} and 0.1 cm s^{-1}, respectively. Negative values are shaded.

Figure 14 shows what happens when a weak localized perturbation is introduced into a marginally unstable zonal flow (such as that profiled in Fig. 16). The disturbance grows slowly to maturity over a period of two years by extracting the excess energy from the shear zone as it traverses the globe. The disturbance remains singular and localized because parameter values lie in the IG range. The currents can only support one vortex if the growth rate of the instability is comparable to the eddy's traversal time, $\pi a \cos 21°/c_\beta$. The eddy in Fig. 14 weakens because the supercritical shear was not maintained.

f. *Genesis of Oval-like vortices*

Strongly unstable currents produce and maintain multiple vortices that are steep and solitary when parameters lie in the IG regime (Fig. 16); the stronger

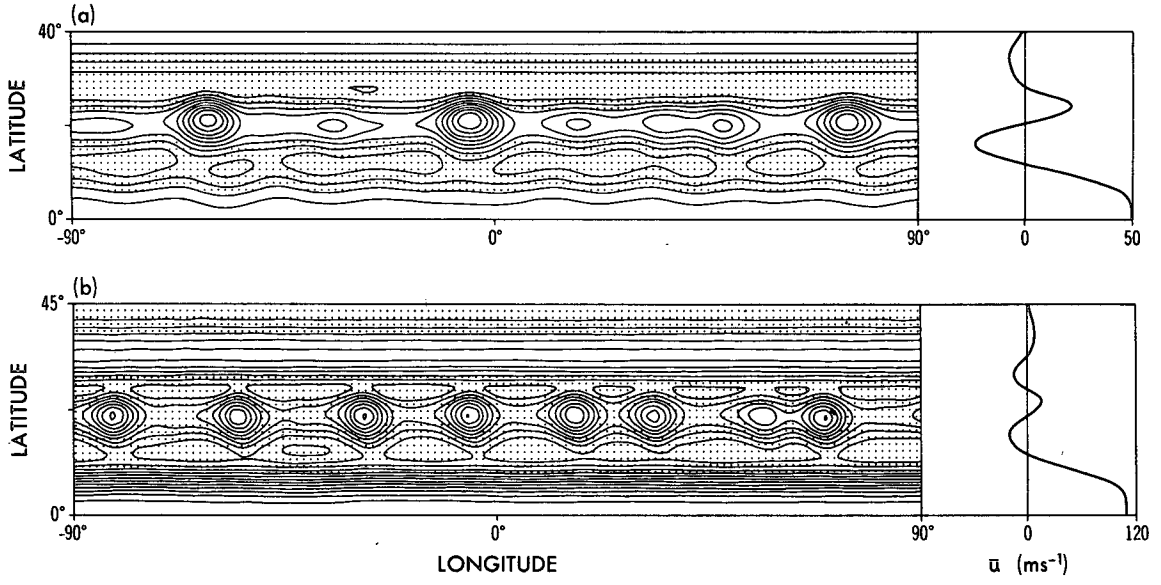

FIG. 16. Solution SW7 and SW8. Anticyclonic vortices produced by (a) moderately, and (b) strongly, unstable anticyclonic shear zones. Contour interval for the free-surface variable $\eta(\lambda, \theta)$ is (a) 1.5 km and (b) 1 km; negative values are shaded. Jovian parameter values are as in Section 2f, with (a) $g = g_J/12$, (b) $g = g_J/10$ and with $\tau = 5 \times 10^6$ s and $\nu = 0.1$ km^2 s^{-1}. Profiles on the rhs give the latitudinal distribution of the zonally averaged zonal flow, with scales of (a) ± 50 m s^{-1} and (b) ± 120 m s^{-1}.

the instability, the greater the number of vortices. The eddies in Fig. 16a resemble the Large Ovals in their solitariness and low number but not in their direction of propagation. Only modification of the System III reference frame can eliminate this difference. These solutions suggest that the Large Ovals are due to a moderate level of instability in the zonal currents. They also suggest that the problem of generating a singular vortex like the GRS is essentially the computational one of dealing with a marginal instability.

When parameters lie in the QG regime ($g > g_J/5$), disturbances take on the customary steady wave form and advective drift rate, for both shear zones and jets (Figs. 17 and 18). In the shear zone, the waves are centered on $\bar{u}(\theta) = 0$ and travel westward at -15 m s^{-1}. In the jet flow, they are centered on the velocity maximum and travel eastward at $+10$ m s^{-1} (Fig. 19). The eddies of the jet instability make little impression on the height field; they are really apparent only in the v-field and in an atmosphere which would "look different" from the other eddies. The wavelike arrangement of the Small Ovals suggests that they are primarily of QG form.

g. Digression on topographic vortices

The instabilities in Figs. 17 and 18 are shown relative to a large, steady singular GRS-scale vortex that is induced by the topographic bump beneath it. This type of vortex, related to the Taylor column, occurs when the bump is wide enough to produce a PG balanced flow, so that no wave dispersion occurs, and when the bump is steep enough to dominate the Sverdrup term. The latter occurs when $(h_B)_y > \beta H f^{-1}$ [see Pedlosky, (1979, Section 5.13)] and the flow then obeys the equations

$$u = -\frac{gh_y}{f}, \quad v = \frac{gh_x}{f}.$$

Thus,

$$u(h_B)_x + v(h_B)_y \approx w \approx 0. \tag{5.1}$$

Theories based on the Taylor column idea have been put forward as explanations of the GRS (see Hide, 1961). They have not been accepted mainly because it is believed that Jupiter's atmosphere and sublayer cannot support any structural inhomogeneities, but also because various analyses have suggested that a Taylor column could not be produced in the presence of stratification and sphericity (e.g., Bannon, 1980). However, all these studies were based on the QG equations which, our analysis suggests, are not appropriate to the GRS problem. As the above solutions show, Taylor columns can exist on the largest planetary scales because dispersive effects are absent from PG balances. Therefore, the Taylor column hypothesis for the GRS is meteorologically tenable but, apparently, constitutionally impossible.

6. Conclusions

The previous solutions show that solitary vortices are the intrinsic mode of the divergence-dominated IG-scale motions and that they maintain their identity over a long period of time, especially when they are of anticyclonic form. On the other hand, QG modes

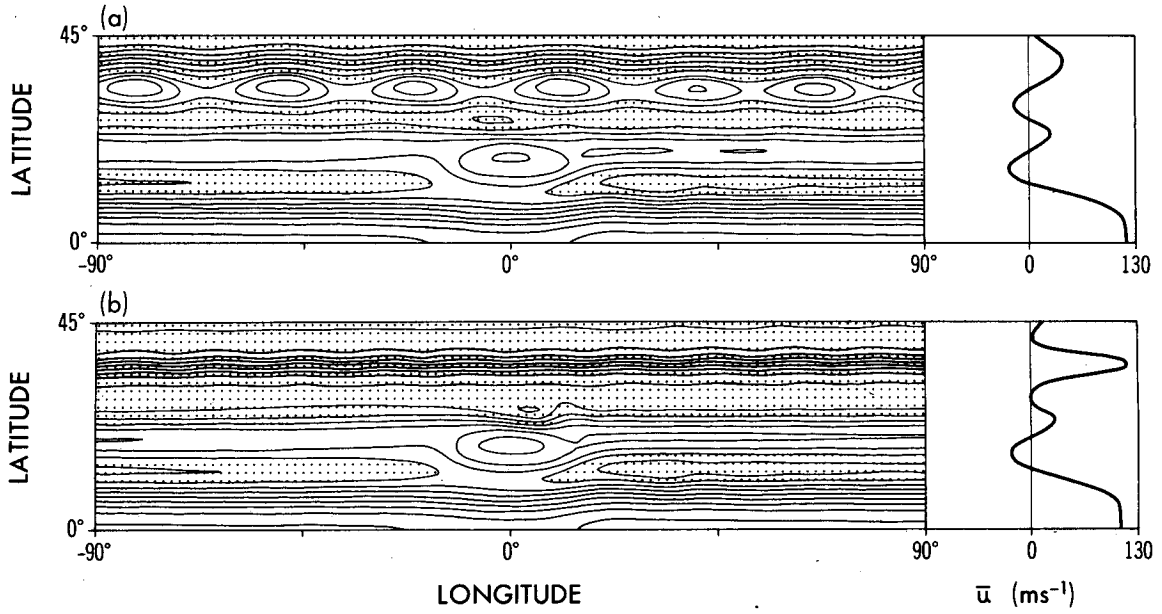

FIG. 17. Solutions SW9 and SW10. The free-surface variables $\eta(\lambda, \theta)$ for the (a) shear zone and (b) jet forms of barotropic instability at QG parameter values ($g = g_f$) and $\theta = 35°$. Also shown is the steady singular anticyclonic vortex produced by an elliptic, truncated Gaussian bump (a mesa) that is 5 km high, 20° long and 8° wide at $\theta = 18°$. Contour interval is 0.4 km but heavier lines near $\theta = 40°$ are spaced at (a) 0.8 km and (b) 1.6 km; negative values are shaded. Zonal velocity profiles are given on the rhs. Jupiter parameter values are as in Section 2f, with $\tau = 2 \times 10^6$ s and $\nu = 0.1$ km^2 s^{-1}.

are primarily wavelike or turbulent and do not display an innate stability nor an anticyclonic over cyclonic preference. The stability of IG vortices appears to be due as much as to their parametric isolation from QG modes as to their internal mechanics. Solutions to the full SW equations suggest that zonal currents also help to isolate the IG vortices by blocking QG wave propagation.

A form of the one-dimensional KdV equation governs the longitudinal evolution of the stable IG vortices, except during collisions when a two-dimensional Jacobian term is activated that prevents soliton forms

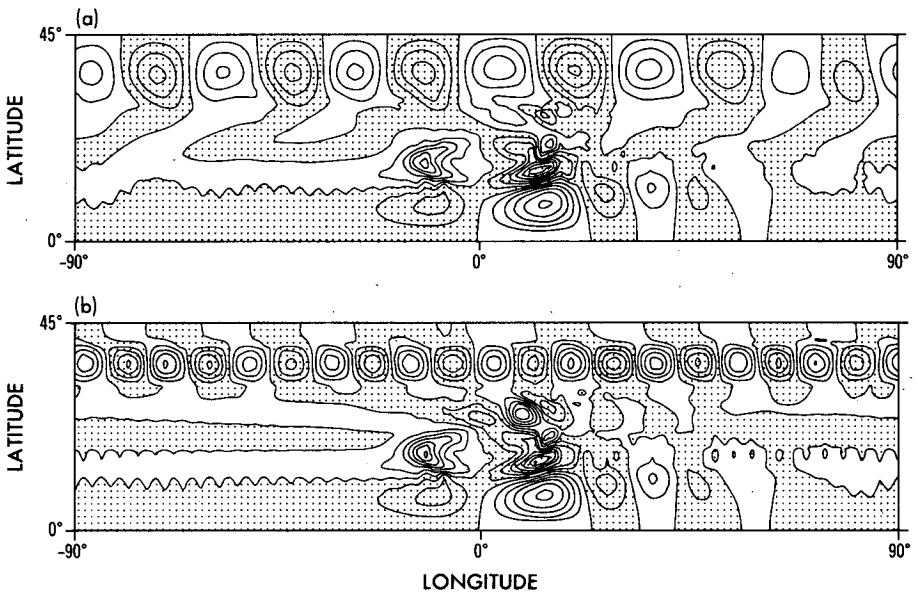

FIG. 18. Solutions SW9 and SW10. The meridional velocity variable $v(\lambda, \theta)$ for the QG solutions of Fig. 17 for (a) shear zone and (b) jet forms of barotropic instability and for the topographic anomaly. Contour interval is 2.5 m s^{-1}; negative values are shaded.

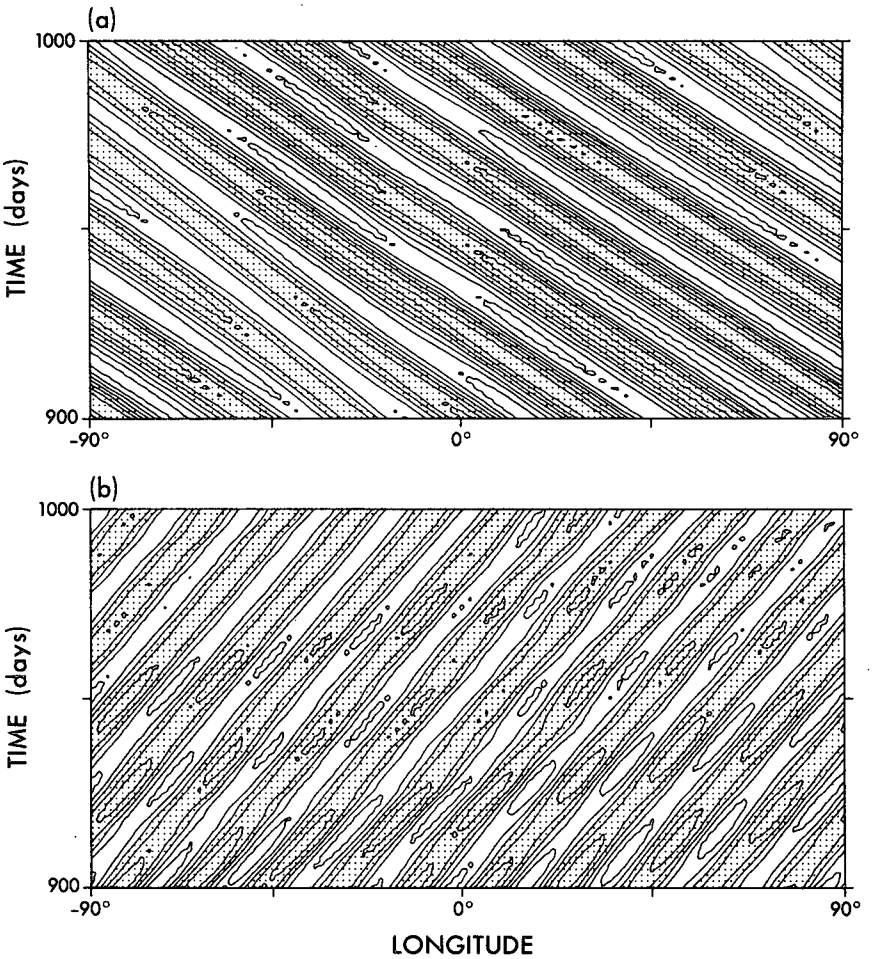

FIG. 19. Solutions SW9 and SW10. The time–longitude plot of the meridional velocity variable $v(\lambda, t)$ at $\theta = 37°$ over 100 days for the QG solutions of Fig. 17 for (a) shear zone and (b) jet forms of barotropic instability. Regularity of eddy amplitude and drift is shown: (a) westward at -15 m s^{-1} and (b) eastward at $+10$ m s^{-1}. Contour interval is (a) 2.5 m s^{-1} and (b) 5 m s^{-1}; negative values are shaded.

of interaction. The coalescence of IG vortices extends, in a discrete and selective way, the inverse cascade of energy that occurs at the smaller QG or two-dimensionally turbulent scales.

The solutions also suggest that Jupiter's Great Red Spot and Large Ovals are the IG vortices produced by weakly and moderately unstable zonal currents. The GRS is then best *defined* as an IG vortex, as its internal processes—the nonlinear divergence and wave propagation—dominate its character; the sources and sinks of energy are secondary aspects. Whether these sources are barotropic, baroclinic or convective is a question that relates mainly to the origin of the object. This view of the GRS is consistent with the (shallow) planetary, as opposed to (deep) solar, view of Jupiter's global circulation. The theory can be tested by looking for evidence of upward (downward) motion in the westward (eastward) half of the GRS.

A crucial question is whether the IG modes favored by the SW model have counterparts in the continuously stratified baroclinic model atmospheres. Preliminary studies suggest they do, if the evolution of the vertical structure of the initial eddy is slow enough to suppress the lateral thermal advection (cf. Gent and McWilliams, 1983). For Jupiter, the study of vertically continuous models is needed to see if stable IG vortices can be developed that have the same amplitude as the GRS or Large Ovals at cloud level and to see whether these eddies originate in barotropically or baroclinically unstable currents (cf. Williams, 1979b). Vertical variations may also lead to slower (or faster) propagation rates and support (or undermine) the usefulness of the System III velocity reference frame. If IG balances exist to any extent for the largest scales of motion in the Earth's atmosphere, then these modes should be more predictable than the smaller QG motions.

Acknowledgments. We are grateful to T. Matsuura (Kyushu University), R. Pacanowski (GFDL) and A. Reif (CDC) for computational assistance, to K. Bryan,

G. Flierl and J. McWilliams for valuable comments, to the GFDL Drafting Group for figure preparation and to B. Williams and J. Kennedy for typing. We also wish to acknowledge the interest shown in our basic ideas by Y. Nogami and T. Asada (Kyoto University), following a personal communication (summer, 1981).

REFERENCES

Anderson, D. L. T., and P. D. Kilworth, 1979: Nonlinear propagation of long Rossby waves. *Deep-Sea Res.*, **26,** 1033–1049.

Arakawa, A., 1966: Computational design for long term integration of the equations of fluid motion. *J. Comput. Phys.*, **1,** 119–143.

Bannon, P. R., 1980: Rotating barotropic flow over finite isolated topography. *J. Fluid Mech.*, **101,** 281–306.

Batchelor, G. K., 1959: *The Theory of Homogeneous Turbulence.* Cambridge University Press, 197 pp.

Beaumont, D. N., 1980: Solitary waves on an unsymmetrical shear flow with applications to Jupiter's Great Red Spot. *Icarus,* **41,** 400–409.

Charney, J. G., and G. R. Flierl, 1981: Oceanic analogues of large scale atmospheric motions. *Evolution of Physical Oceanography,* B. A. Warren and C. Wunsch, Eds., The MIT Press, 504–548.

Flierl, G. R., M. E. Stern and J. B. Whitehead, Jr., 1983: The physical significance of modons: Laboratory experiments and general integral constraints. *Dyn. Atmos. Oceans,* **7,** 233–263.

Gent, P. R., and J. C. McWilliams, 1983: Regimes of validity for balanced models. *Dyn. Atmos. Oceans,* **7,** 167–183.

Hide, R., 1961: Origin of Jupiter's Great Red Spot. *Nature,* **190,** 895–896.

Hunt, G., and P. Moore, 1981: *Jupiter.* Rand McNally, 96 pp.

Ingersoll, A. P., and P. G. Cuong, 1981: Numerical model of long-lived Jovian vortices. *J. Atmos. Sci.*, **38,** 2067–2076.

Kuo, H-L., 1959: Finite amplitude three-dimensional harmonic waves on a spherical earth. *J. Meteor.*, **16,** 524–534.

Matsuura, T., and T. Yamagata, 1982: On the evolution of nonlinear planetary eddies larger than the radius of deformation. *J. Phys. Oceanogr.*, **12,** 440–456.

Maxworthy, T., and L. G. Redekopp, 1976: A solitary wave theory of the Great Red Spot and other observed features of the Jovian atmosphere. *Icarus,* **29,** 261–271.

McWilliams, J. C., and N. J. Zabusky, 1982: Interactions of isolated vortices. *Geophys. Astrophys. Fluid Dyn.*, **19,** 207–227.

Meyers, G., 1979: On the annual Rossby wave in the tropical North Pacific Ocean. *J. Phys. Oceanogr.*, **9,** 663–674.

Miles, J. W., 1980: Solitary waves. *Annual Review of Fluid Mechanics,* Vol. 12, Annual Reviews, Inc., 11–43.

Mitchell, J. L., R. F. Beebe, A. P. Ingersoll and G. W. Garneau, 1981: Flow fields within Jupiter's Great Red Spot and White Oval B.C. *J. Geophys. Res.*, **86,** 8751–8757.

Pedlosky, J., 1979: *Geophysical Fluid Dynamics.* Springer-Verlag, 624 pp.

Phillips, N. A., 1963: Geostrophic motion. *Rev. Geophys.*, **1,** 123–176.

Rhines, P. B., 1977: The dynamics of unsteady currents. *The Sea,* Vol. 6, E. D. Goldberg, I. N. McCave, J. J. O'Brien and J. H. Steele, Eds., Wiley, 189–318.

Sadourney, R., 1975: Compressible model flows on the sphere. *J. Atmos. Sci.*, **32,** 2103–2110.

Thompson, P. D., 1948: The propagation of permanent type waves in horizontal flow. *J. Meteor.*, **5,** 166–168.

White, W. B., 1977: Annual forcing of baroclinic long waves in the tropical North Pacific. *J. Phys. Oceanogr.*, **7,** 50–61.

Williams, G. P., 1978: Planetary circulations: 1. Barotropic representation of Jovian and terrestrial turbulence. *J. Atmos. Sci.*, **35,** 1399–1426.

——, 1979a: Planetary circulations: 2. The Jovian quasi-geostrophic regime. *J. Atmos. Sci.*, **36,** 932–968.

——, 1979b: Ultra-long baroclinic waves and Jupiter's Great Red Spot. *J. Meteor. Soc. Japan,* **57,** 196–198.

——, and J. L. Holloway, Jr., 1982: The range and unity of planetary circulations. *Nature,* **297,** 295–299.

Winant, C. D., and F. K. Browand, 1974: Vortex pairing: The mechanism of turbulent mixing-layer growth at moderate Reynolds number. *J. Fluid Mech.*, **63,** 237–255.

Yamagata, T., 1980: On the nonlinear modulation of planetary topographic waves in a rotating stratified ocean. *Geophys. Astrophys. Fluid Dyn.*, **16,** 35–54.

——, 1982: On nonlinear planetary waves: A class of solutions missed by the traditional quasi-geostrophic approximation. *J. Oceanogr. Soc. Japan,* **38,** 236–244.